

Constraining the Higgs self-couplings at e^+e^- colliders

Fabio Maltoni,^a Davide Pagani,^b Xiaoran Zhao^a

^a*Centre for Cosmology, Particle Physics and Phenomenology (CP3), Université catholique de Louvain, B-1348 Louvain-la-Neuve, Belgium*

^b*Technische Universität München, James-Frank-Str. 1, D-85748 Garching, Germany*

E-mail: fabio.maltoni@uclouvain.be, davide.pagani@tum.de,
xiaoran.zhao@uclouvain.be

ABSTRACT: We study the sensitivity to the shape of the Higgs potential of single, double, and triple Higgs production at future e^+e^- colliders. Physics beyond the Standard Model is parameterised through the inclusion of higher-dimensional operators $(\Phi^\dagger\Phi - v^2/2)^n/\Lambda^{(2n-4)}$ with $n = 3, 4$, which allows a consistent treatment of independent deviations of the cubic and quartic self-couplings beyond the tree level. We calculate the effects induced by a modified potential up to one loop in single and double Higgs production and at the tree level in triple Higgs production, for both Z boson associated and W boson fusion production mechanisms. We consider two different scenarios. First, the dimension six operator provides the dominant contribution (as expected, for instance, in a linear effective-field-theory (EFT)); we find in this case that the corresponding Wilson coefficient can be determined at $\mathcal{O}(10\%)$ accuracy by just combining accurate measurements of single Higgs cross sections at $\sqrt{s} = 240\text{--}250$ GeV and double Higgs production in W boson fusion at higher energies. Second, both operators of dimension six and eight can give effects of similar order, *i.e.*, independent quartic self-coupling deviations are present. Constraints on Wilson coefficients can be best tested by combining measurements from single, double and triple Higgs production. Given that the sensitivity of single Higgs production to the dimension eight operator is presently unknown, we consider double and triple Higgs production and show that combining their information colliders at higher energies will provide first coarse constraints on the corresponding Wilson coefficient.

¹Preprint: MCnet-18-02, CP3-18-17, TUM-HEP-1132/18.

Contents

1	Introduction	1
2	Theoretical setup	5
2.1	Notation and parametrisation of New Physics effects	5
3	Single, double and triple Higgs production: \bar{c}_6 and \bar{c}_8 dependence	7
3.1	Single Higgs production	8
3.2	Double Higgs production	10
3.3	Triple Higgs production	16
4	Bounds on the Higgs self-couplings	17
4.1	Single Higgs production	18
4.2	Double Higgs production	21
4.3	Triple Higgs production	23
4.4	Combined bounds	25
5	Conclusions	28
A	One-loop renormalisation in double Higgs production in EFT	31
B	One-loop amplitudes via form factors	33
C	Perturbative limits on \bar{c}_6 and \bar{c}_8 in double Higgs production	39

1 Introduction

In the Standard Model (SM), the breaking of the electroweak symmetry, $SU(2)_L \times U(1)_Y \rightarrow U(1)_{\text{QED}}$, is induced by the potential:

$$V^{\text{SM}}(\Phi) = -\mu^2(\Phi^\dagger\Phi) + \lambda(\Phi^\dagger\Phi)^2, \quad (1.1)$$

where Φ is the Higgs doublet and the parameters μ and λ depend on the vacuum expectation value of the Higgs field v (or equivalently, the Fermi constant G_F) and the Higgs boson mass m_H , *i.e.*, $\mu^2 = m_H^2/2$ and $\lambda = m_H^2/(2v^2)$. The form of eq. (1.1) is dictated by the symmetries of the SM and the requirement of renormalisability. It is therefore a firm prediction of the SM that, once m_H is known, the Higgs boson (H) self interactions are uniquely determined; $\lambda_3^{\text{SM}} = \lambda_4^{\text{SM}} = \lambda$, where $\lambda_3^{\text{SM}}(\lambda_4^{\text{SM}})$ is the factor in front of the vH^3 ($H^4/4$) interaction in the SM Lagrangian after ElectroWeak Symmetry Breaking (EWSB). Since its discovery in 2012 [1, 2] a wealth of information has been accumulated on the scalar particle at 125 GeV of mass. Its couplings to vector bosons and third generation

fermions [3] are so far all compatible with the SM expectations. However, no confirmation on the SM form of the Higgs potential is yet available from collider experiments. The reason of this lies in the intrinsic difficulty of accessing the relevant information experimentally.

Determining the form of the Higgs potential necessarily implies measuring the strength of the Higgs three- and four- (and possibly higher) point self-couplings. This is a challenging task at colliders for several reasons. As mentioned above, the self-couplings are proportional to λ , which in the SM is about $1/8$ and therefore rather weak, *i.e.* of the same order of the Higgs couplings to the vector bosons and significantly smaller than the Yukawa coupling to the top quark. In addition, for a direct sensitivity on $\lambda_3(\lambda_4)$, processes featuring at least three(four) Higgs bosons need to be considered, namely double(triple) Higgs production. As a result, effects associated to the self-couplings in the range of the SM values are in general very small. This simple fact has two immediate implications. First, one will need considerable statistics to be collected at the LHC Run II and III and in future electron-positron colliders before reaching the sensitivity to values close the SM predictions. Second, the precision of the experimental determinations of the self-couplings will critically depend on that of the other Higgs boson couplings entering the same process (or more in general the observable) under consideration. For example, at the LHC the largest production rate is due to gluon fusion processes via a top-quark loop. While the leading contribution from the top-quark Yukawa coupling y_t scales as y_t^4 , the leading contribution from the Higgs self-coupling scales as $(\lambda_3)^2$ and is kinematically suppressed at large $m(HH)$ invariant-mass values.

Many studies have been performed for the LHC at $\sqrt{s} = 13$ TeV aiming to directly access λ_3 from double Higgs production measurements [4–21]. However, due to the complexity of the corresponding realistic experimental setups, it is still unclear what is the final precision that could be achieved on the determination of λ_3 . At the moment the strongest experimental bounds on λ_3 (from non-resonant double-Higgs production) have been obtained in the CMS analysis for the $b\bar{b}\gamma\gamma$ signature [22]. Exclusion limits on λ_3 have been found to strongly depend on the value of the top Yukawa coupling y_t . In particular, in the case of an SM y_t value, order $\lambda_3 < -9 \lambda_3^{\text{SM}}$ and $\lambda_3 > 15 \lambda_3^{\text{SM}}$ limits are obtained. According to optimistic *experimental* projection studies [23], even with the high luminosity (HL) option of 3000 fb^{-1} it may be possible to exclude values only in the range $\lambda_3 < -1.3 \lambda_3^{\text{SM}}$ and $\lambda_3 > 8.7 \lambda_3^{\text{SM}}$.

Concerning the quadrilinear coupling λ_4 , it is instead incontrovertibly clear that the possibility of constraining λ_4 via the measurement of triple Higgs production at the LHC is quite bleak [24–27]. Even at a future 100 TeV proton-proton collider only loose bounds may be obtained with a considerable amount of integrated luminosity [28–30].

Additional and complementary strategies for the determination of λ_3 and λ_4 are therefore desirable not only at the moment but also for the (near) future. To this purpose, a lot of new results have recently appeared aiming to access λ_3 via indirect loop-induced effects. This idea has been pioneered by McCullough in the context of e^+e^- colliders [31], where loop-induced effects in single-Higgs production have been investigated for ZH associated production [32–34]. A first evaluation of analogous loop effects at the LHC has been pre-

sented in ref. [35] for $gg \rightarrow H \rightarrow \gamma\gamma$. At the same time, the complete set of (one- and two-) loop computations for all relevant single-Higgs observables at the LHC together with the proposal of combining inclusive and differential observables, has been put forward in [36]. Since then several studies have appeared: the computation of the factorisable QCD corrections to the single-Higgs EW production at the LHC [37], two-loop effects in precision EW observables [38, 39] and, more recently, further investigations on the impact of the differential information and the relevance of SM electroweak corrections [40]. Furthermore, global analyses in the context of an SMEFT (SM-EFT) have also been presented for present and future measurements at the LHC [41] and even for the case of future e^+e^- colliders [42, 43]. On the other hand, in these works, effects of λ_4 have been either ignored, being irrelevant for the calculation considered, or assumed to be determined in turn by the λ_3 value.

In the present work we investigate for the first time the (combined) sensitivity to both the λ_3 and λ_4 self-couplings in (multi-)Higgs production at future e^+e^- colliders. We consider H , HH , and HHH production both in association with a Z boson or via W -boson fusion (WBF) [44]. These processes are listed in Tab. 1, where we have also specified at

Process	λ_3	λ_4
$ZH, \nu_e \bar{\nu}_e H$ (WBF)	one-loop	two-loop
$ZHH, \nu_e \bar{\nu}_e HH$ (WBF)	tree	one-loop
$ZHHH, \nu_e \bar{\nu}_e HHH$ (WBF)	tree	tree

Table 1: Processes considered in this work and the order at which the λ_3 and λ_4 dependence appears. We do not calculate two-loop effects, but we do calculate one-loop effects for both single and double Higgs production.

which level in perturbation theory the λ_3 and λ_4 dependence appears (we do not calculate two-loop effects in this work). In particular, we perform the computation of one-loop effects in single and (for the first time) double Higgs production. The former pose no theoretical challenge, confirm the results of [31, 43] (and *mutatis mutandis*, of [36, 37]); they are presented here for completeness and are also used in our analysis. On the other hand, one-loop effects in double Higgs production can be computed only within a complete and consistent EFT approach, where UV renormalisation can be performed. To this purpose, we work in a theoretical and computational framework where the cubic and quartic couplings can independently deviate from the SM predictions and loop computations can be consistently performed. Specifically, we add the two higher-dimensional operators $c_{2n}(\Phi^\dagger\Phi - v^2/2)^n/\Lambda^{(2n-4)}$ with $n = 3, 4$ to the SM Lagrangian, where the presence of the “ $-v^2$ ” term considerably simplifies the technical steps of the one-loop calculation in double Higgs production. On the other hand, Wilson coefficients in this basis or in the standard $c'_{2n}(\Phi^\dagger\Phi)^n/\Lambda^{(2n-4)}$ parameterisation can be easily related at any perturbative order and also after the running to a different scale. While the c'_{2n} coefficient are more suitable for the matching to a UV-complete model, the c_{2n} ones feature simple relations to Higgs self-couplings, and are more convenient for phenomenological predictions such as

those performed here for (multi-)Higgs production. Independently from the choice of the basis, it will be clear in the text that the Wilson coefficients c'_6 and c'_8 , or c_6 and c_8 , are the relevant parameter to be considered and not directly the λ_3 and λ_4 couplings.

By comparing and combining the direct and indirect sensitivities on the Higgs self-couplings that could be obtained at future e^+e^- colliders (CEPC[45], FCC-ee[46], ILC[47] and CLIC[48, 49]) running at different energies and luminosities, we explore the final reach of such colliders to constrain the Higgs potential. In general, we assume that BSM effects due to the Higgs interactions with the other SM particles are negligible w.r.t. those induced by self interactions. In practice, we work under the same assumptions of the first calculations of one-loop λ_3 effects in single Higgs production at e^+e^- [31] or proton–proton collisions [35, 36], which represented an unavoidable input for the analyses considering a more general class of BSM scenarios [41–43]. On the other hand, precisely one of these recent global analyses, ref. [43], has shown that in high-energy e^+e^- collisions, where ZHH and WBF HH production are kinematically available, working with our assumption or allowing for additional BSM effects does not affect the constraints that can be obtained for the trilinear Higgs self-coupling, thus justifying our working assumption. In this work we will investigate the precision that can be achieved on the trilinear Higgs self-coupling, not only when it is close to its SM value, *i.e.*, we will explore also regimes where its effects entering via loop corrections can be relevant also in double-Higgs production. Moreover, these loop corrections, similarly to $ZHHH$ and WBF HHH production at the Born level, involve effects due to the quadrilinear Higgs self-coupling. We will investigate the constraints that can be set on this coupling under two different assumptions. In the first, we consider the case of a well behaving EFT expansion, where dimension-eight operators induce effects smaller than dimension-six ones. In other words, the value of the trilinear coupling automatically sets also the value of the quadrilinear coupling. In the second, we lift this assumptions and we allow for independent trilinear and quadrilinear couplings, namely, we allow for similar effects from $(\Phi^\dagger\Phi)^3$ and $(\Phi^\dagger\Phi)^4$ operators.

The paper is organised as follows. In section 2 we introduce the notation and we discuss the EFT framework used in our calculation. The details concerning the definition of the renormalisation scheme at one loop and all the necessary counterterms for the calculation performed here are given in Appendix A. In section 3 we provide the predictions for cross sections of single, double and triple Higgs production at different energies, discussing their dependence on the c_6 and c_8 parameters. The one-loop calculations in single and double Higgs production are performed via one-loop form factors, the explicit results for which are provided in Appendix B. In section 4 we determine the reach of several experimental setups at future e^+e^- colliders for constraining the cubic and quartic couplings; both individual and combined results from single, double and triple Higgs production are scrutinised. The maximum c_6 and c_8 values beyond which perturbative convergence cannot be trusted are derived in Appendix C. We draw our conclusions in section 5.

2 Theoretical setup

2.1 Notation and parametrisation of New Physics effects

In this work we are interested to the effect induced by the modification $V^{\text{SM}}(\Phi) \rightarrow V(\Phi)$ defined as

$$V(\Phi) = V^{\text{SM}}(\Phi) + V^{\text{NP}}(\Phi), \quad \Phi = \begin{pmatrix} G^+ \\ \frac{1}{\sqrt{2}}(v + H + iG^0) \end{pmatrix}, \quad (2.1)$$

where the New Physics (NP) modifications of the potential are all included in V^{NP} and the symbol Φ denotes the Higgs doublet. The term V^{SM} has already been defined in eq. (1.1).

Following the convention of ref. [50], the most general form of V^{NP} that is invariant under $SU(2)$ symmetry can be written as

$$V^{\text{NP}}(\Phi) \equiv \sum_{n=3}^{\infty} \frac{c_{2n}}{\Lambda^{2n-4}} \left(\Phi^\dagger \Phi - \frac{1}{2}v^2 \right)^n. \quad (2.2)$$

It is important to specify from the beginning why for our calculation it is convenient to parametrise the NP contributions as done in eq. (2.2) and not using the standard EFT parameterisation

$$V_{\text{std}}^{\text{NP}}(\Phi) \equiv \sum_{n=3}^{\infty} \frac{c'_{2n}}{\Lambda^{2n-4}} \left(\Phi^\dagger \Phi \right)^n. \quad (2.3)$$

The advantages of the parametrisation in eq. (2.2) w.r.t the one in eq. (2.3) are due to the fact that after EWSB any $(\Phi^\dagger \Phi)^n$ originates H^i terms with $1 \leq i \leq 2n$, while any $(\Phi^\dagger \Phi - \frac{1}{2}v^2)^n$ originates H^i terms only with $n \leq i \leq 2n$. In other words, at tree-level, the trilinear Higgs self-coupling receives modifications only from c_6 and the quadrilinear only from c_6 and c_8 . Needless to say, when they are summed to V^{SM} , equations (2.2) and (2.3) not only refer to the same quantity parametrised in a different way ($V^{\text{SM}} + V_{\text{std}}^{\text{NP}} = V^{\text{SM}} + V^{\text{NP}}$), but they are also fully equivalent for any truncation of the series at a given order n .

Writing $V^{\text{SM}}(\Phi) + V^{\text{NP}}(\Phi)$ after EWSB as

$$V(H) = \frac{1}{2}m_H^2 H^2 + \lambda_3 v H^3 + \frac{1}{4}\lambda_4 H^4 + \lambda_5 \frac{H^5}{v} + O(H^6) \quad (2.4)$$

allows to define the self-couplings λ_n , which can be parametrised by the quantities¹

$$\kappa_3 \equiv \frac{\lambda_3}{\lambda_3^{\text{SM}}} = 1 + \frac{c_6 v^2}{\lambda \Lambda^2} \equiv 1 + \bar{c}_6, \quad (2.5)$$

$$\kappa_4 \equiv \frac{\lambda_4}{\lambda_4^{\text{SM}}} = 1 + \frac{6c_6 v^2}{\lambda \Lambda^2} + \frac{4c_8 v^4}{\lambda \Lambda^4} \equiv 1 + 6\bar{c}_6 + \bar{c}_8, \quad (2.6)$$

$$\kappa_5 \equiv \frac{\lambda_5}{\lambda} = \frac{3c_6 v^2}{4\lambda \Lambda^2} + \frac{2c_8 v^4}{\lambda \Lambda^4} + \frac{c_{10} v^6}{\lambda \Lambda^6} \equiv \frac{3}{4}\bar{c}_6 + \frac{1}{2}\bar{c}_8 + \bar{c}_{10}. \quad (2.7)$$

¹Note that κ_3 and κ_4 are defined differently than κ_5 . The former are the ratios of the trilinear and quadrilinear couplings with their SM values. The latter is the value normalised to λ , being a tree-level H^5 interaction not present in the SM.

where $\lambda_3^{\text{SM}}(\lambda_4^{\text{SM}})$ is the value of $\lambda_3(\lambda_4)$ in the SM and reads

$$\lambda_3^{\text{SM}} = \lambda_4^{\text{SM}} = \lambda = \frac{m_H^2}{2v^2}. \quad (2.8)$$

In other words, \bar{c}_6, \bar{c}_8 and \bar{c}_{10} are c_6, c_8 and c_{10} normalised in such a way that can be easily related to κ_3, κ_4 and κ_5 . In particular

$$\bar{c}_6 \equiv \frac{c_6 v^2}{\lambda \Lambda^2} = \kappa_3 - 1, \quad (2.9)$$

$$\bar{c}_8 \equiv \frac{4c_8 v^4}{\lambda \Lambda^4} = \kappa_4 - 1 - 6(\kappa_3 - 1). \quad (2.10)$$

Eqs. (2.5) and (2.6) make two important points manifest. First, while the trilinear coupling only depends on c_6 , the quadrilinear depends on both c_6 and c_8 . Thus, in a well-behaved EFT, where the effects of higher dimensional operators are systematically suppressed by a large scale, one expects deviations both in κ_3 and κ_4 and such that $(\kappa_4 - 1) \simeq 6(\kappa_3 - 1)$, see also eq. (2.10). Second, κ_3 and κ_4 do not depend on any c_{2n} coefficient with $n > 4$, without any assumption on the c_{2n} values with $n > 4$. In other words, for the study of trilinear and quadrilinear Higgs self-couplings *at the tree level*, only the c_6 and c_8 Wilson coefficients are relevant. On the other hand, *at one-loop level* also c_{10} is in principle needed.

As already mentioned in the introduction, in this paper we will calculate one-loop corrections to double Higgs production, taking into account both c_6 and c_8 effects. In general, when loop corrections are calculated and c_{2n} coefficients themselves are renormalised, the parametrisation of eq. (2.2) is convenient also for other reasons that are particularly relevant when the Wilson coefficients are renormalised. At variance with eq. (2.3), the values of the coefficients c_{2n} influence only the value of the Higgs self-couplings; they do not alter the SM relations among m_H, v, μ and λ

$$\mu^2 = \frac{m_H^2}{2}, \quad (2.11)$$

$$\lambda = \frac{m_H^2}{2v^2}. \quad (2.12)$$

This is convenient because the physical quantities are m_H and v and not μ and λ , while using eq. (2.3) one has to determine before μ and λ and then the self-couplings (see Appendix A of [36]). Especially, and this is the main motivation for this work, thanks to eqs. (2.11) and (2.12) the modification $V^{\text{SM}}(\Phi) \rightarrow V^{\text{SM}}(\Phi) + V^{\text{NP}}(\Phi)$ allows to keep the SM relations between the renormalisation constants and the definition of the renormalisation counterterms as done in ref. [51]. On the other hand, the explicit insertion of v^2 in eq. (2.2) deserves a particular attention for the renormalisation procedure and leads to additional counterterms. All the necessary ingredients for the calculations performed here are provided in Appendix A.

It is important to note that the coefficients c_{2n} in eq. (2.2) and c'_{2n} in eq. (2.3) are connected by very simple relations and can be converted ones into the others at any step of the calculation. Thus, our calculation is fully equivalent to using the c'_{2n} coefficients and

renormalising them in the $\overline{\text{MS}}$ scheme (see Appendix A). Via the simple tree-level relations among c_{2n} and c'_{2n} coefficients one can convert results at any order from one convention to the other, including the renormalisation-group equations. As already said, while c'_{2n} coefficients are more suitable for the matching to a UV-complete model, the c_{2n} coefficients are more convenient for one-loop calculations of hard-scattering matrix elements such as those performed here for double Higgs production. Independently from the basis choice, the NP effects should be parametrised via c'_6 and c'_8 , or c_6 and c_8 , rather than directly through the λ_3 and λ_4 couplings. The reason is that the individual Wilson coefficients are the quantities entering the renormalisation procedure, and c'_6 , or equivalently c_6 , is affecting both λ_3 and λ_4 values. In the following we will mainly parametrise NP via the \bar{c}_{2n} coefficients, which are simply related to both c_{2n} and κ_n (see eqs.(2.5)-(2.10)).

3 Single, double and triple Higgs production: \bar{c}_6 and \bar{c}_8 dependence

In this section we describe the calculations for single, double and triple Higgs production via WBF, the $e^+e^- \rightarrow \nu_e \bar{\nu}_e H(H(H))$ processes, or in association with a Z boson, the $e^+e^- \rightarrow ZH(H(H))$ processes. We will denote the latter also as ZH^n . Besides the ZH^n and WBF production modes, at e^+e^- colliders there are other possibly relevant processes such as $t\bar{t}H^n$, Z -boson-fusion (ZBF) or loop-induced H^n production via photon fusion [50] from the initial-state radiation. However, these processes have considerably smaller cross sections than WBF or ZH^n production modes, so we do not consider them in our analysis. Part of them have been considered in ref. [43] and their impact has been indeed found to be negligible.

While triple Higgs production processes are calculated at the Born level, for both single and double Higgs production we take into account also one-loop corrections involving the additional \bar{c}_6 and \bar{c}_8 dependence. The sensitivity on \bar{c}_6 and \bar{c}_8 , and in turn on κ_3 and κ_4 , depends on the multiplicity of Higgs bosons in the final state and the numbers of loop corrections considered, as summarised in Tab. 1. We expect complementary information from ZH^n and WBF, when the different collider energies of the possible future e^+e^- colliders are considered. While the cross section of ZH^n is maximal for energies slightly larger than its production threshold, the WBF cross section grows with the energy. Moreover, based on results in refs. [31, 36, 37, 40, 43], in ZH^n production we expect a strong dependence of the Higgs self-coupling effects from loop corrections, with larger effects at lower energies. On the contrary, in WBF this energy-dependence is expected to be much smaller.

It is important to note that ZH^n and WBF cross sections, and in turn their sensitivity on \bar{c}_6 and \bar{c}_8 , depend on beam polarisations, which can be tuned at linear colliders.² First of all, WBF contributes only via the LR polarisations,³ since W -boson couples only to the left-chirality fermions. Conversely, the ZH^n processes can also originate from RL polarisations (right-handed e^- , left-handed e^+), also denoted as $P(e^-, e^+) = (1.0, -1.0)$.

²Due to the Sokolov Ternov effect [52], the tuning of beam polarisations is much more difficult in circular colliders.

³Here, as in the following, we are neglecting power-suppressed terms that depend on the mass of the electron.

On the other hand, results for RL polarisations can be easily obtained from those with LR via the relation

$$\sigma_{RL} = \sigma_{LR} \left(\frac{2 \sin^2 \theta_W}{1 - 2 \sin^2 \theta_W} \right)^2 \approx 0.65 \sigma_{LR}, \quad (3.1)$$

In all our calculations we use following input parameters [53]

$$\begin{aligned} G_\mu &= 1.166\,378\,7 \times 10^{-5} \text{ GeV}^{-2}, \quad m_W = 80.385 \text{ GeV}, \quad m_Z = 91.1876 \text{ GeV} \\ m_H &= 125 \text{ GeV}, \quad m_t = 173.21 \text{ GeV}, \end{aligned} \quad (3.2)$$

We assume \bar{c}_6 and \bar{c}_8 measured at the scale $\mu_r = 2m_H$, which therefore we will also use as $\overline{\text{MS}}$ renormalisation scale for \bar{c}_6 in the double Higgs computation.

The WBF production modes feature the same final states of ZH^n production with $Z \rightarrow \nu_e \bar{\nu}_e$ decays. The latter are not considered as part of the WBF contribution in our calculation. Although NLO EW corrections in the SM would jeopardise the gauge invariance of this classification at the amplitude level [54], this is not the case for the one-loop corrections induced by additional c_{2n} interactions, which is the kind of effects we consider in this work on top of LO effects, as better specified later in eqs. (3.5) and (3.11). Moreover, the interference of ZH^n -type diagrams with “genuine” WBF configurations is negligible

3.1 Single Higgs production

In this section we briefly (re)-describe the calculation of loop-induced effects from $\bar{c}_6(\kappa_3)$ in ZH and single-Higgs WBF production at e^+e^- colliders (representative diagrams are shown in Fig. 1). We introduce the notation that will be generalised to the case of double Higgs and triple Higgs production and we show how it is related to the previous calculations [31, 36, 40, 43].

For both WBF and ZH production channels no Higgs self-coupling contributes at the tree level. On the other hand, one-loop corrections depends on the trilinear Higgs self-coupling, but not on the quartic. Thus, while the LO cross section $\sigma_{\text{LO}}(H)$ is only of SM origin, NLO predictions includes also effects from \bar{c}_6 :

$$\sigma_{\text{NLO}}(H) = \sigma_{\text{LO}}(H) + \sigma_{1\text{-loop}}(H), \quad (3.3)$$

$$\sigma_{\text{LO}}(H) = \sigma_{\text{LO}}^{\text{SM}}(H), \quad (3.4)$$

$$\sigma_{1\text{-loop}}(H) = \sigma_0 + \sigma_1 \bar{c}_6 + \sigma_2 \bar{c}_6^2, \quad (3.5)$$

where $\sigma_{1\text{-loop}}$ involves one-loop corrections of both SM origin and induced by c_6 . The quantity σ_0 consists of the NLO EW corrections from the SM, σ_1 represents the leading contribution in the EFT expansion (order $(v/\Lambda)^2$), while σ_2 is of order $(v/\Lambda)^4$, also arising from one-loop corrections.⁴ Note that within our choice of operators there is no contribution

⁴Whenever we refer to NLO EW corrections of SM origin, those include also real emissions of photons. On the contrary, one-loop effects induced by c_{2n} are infrared safe and involve just virtual corrections. Needless to say, at one-loop, NLO QCD corrections are vanishing for the processes considered in this paper.

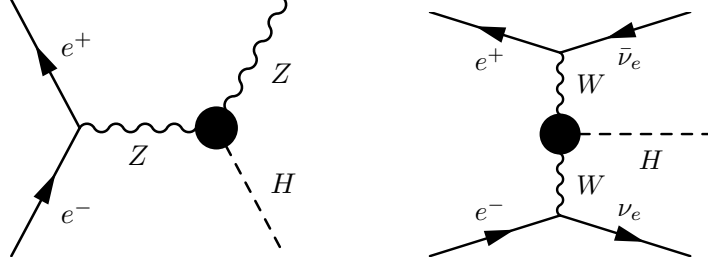


Figure 1: Feynman diagrams for single Higgs production. The black blob corresponds to the one-loop HVV form factors.

proportional to \bar{c}_8 or any other c_{2n} coefficient in this expansion, meaning that eq. (3.5) is actually exact; no other terms can enter at all even for higher orders in the (v/Λ) expansion. Furthermore, we remind that, at variance with the case of double Higgs production, in single Higgs production at one-loop the anomalous coupling approach (κ_3) is fully equivalent to the calculation in the EFT (\bar{c}_6).

For our phenomenological study we ignore the SM NLO EW corrections [54, 55]. Our main focus is not the precise determination of \bar{c}_6 , but the study of its impact via its leading contributions. As discussed in detail in ref. [40], SM NLO EW corrections have a tiny impact on the extraction of the value of \bar{c}_6 and do not affect the accuracy of the determination of \bar{c}_6 . Therefore, we consider \bar{c}_6 effects at one loop via the following approximation

$$\sigma_{\text{NLO}}^{\text{pheno}}(H) = \sigma_{\text{LO}} + \sigma_1 \bar{c}_6 + \sigma_2 \bar{c}_6^2. \quad (3.6)$$

With this approximation, the sensitivity to the trilinear coupling can be expressed via the ratio

$$\delta\sigma(H) \equiv \frac{\sigma_{\text{NLO}}^{\text{pheno}} - \sigma_{\text{LO}}}{\sigma_{\text{LO}}} = \frac{\sigma_1 \bar{c}_6 + \sigma_2 \bar{c}_6^2}{\sigma_{\text{LO}}} = (\kappa_3 - 1)C_1 + (\kappa_3^2 - 1)C_2, \quad (3.7)$$

$$C_2 = \delta Z_H^{\text{SM},\lambda}, \quad (3.8)$$

where we have expressed the $\sigma_i/\sigma_{\text{LO}}$ ratios directly⁵ using the symbols C_1 and C_2 introduced in ref. [36]. C_1 denotes the one-loop virtual contribution involving one triple Higgs vertex, while C_2 originates from the Higgs wave-function renormalisation constant (see eqs. (A.2), (A.14) and (A.17)), which is the only source of \bar{c}_6^2 and thus κ_3^2 dependence at one loop level. Both C_1 and C_2 are independently UV-finite and, for simplicity, we choose not to resum higher-orders contributions to the wave function, at variance with ref. [36]. Indeed, given the results already presented in ref. [31], we expect to bound κ_3 close to the SM ($\kappa_3 = 1$) and in this scenario such a resummation would not make a noticeable difference anyway. Moreover, even considering κ_3 in the range $|\kappa_3| < 6$ from ref. [56], the difference between the formula in eq. (3.7) and including the resummed higher-order contributions to Z_H is below 1% (see also ref. [40]). Considering C_2 in eq. (3.8), the difference w.r.t. the definition in ref. [36] is only due to this choice, however, in the limit $\bar{c}_6 \rightarrow 0$ ($\kappa_3 \rightarrow 1$) the

⁵Note that $\kappa_3^2 - 1 = (\kappa_3 - 1)^2 + 2(\kappa_3 - 1)$, so $\sigma_2 = C_2\sigma_{\text{LO}}$ and $\sigma_1 = (C_1 + 2C_2)\sigma_{\text{LO}}$

two different definitions are equivalent as can be seen from the value of C_2 :

$$C_2 = \delta Z_H^{\text{SM},\lambda} \equiv -\frac{9}{16} \frac{G_\mu m_H^2}{\sqrt{2}\pi^2} \left(\frac{2\pi}{3\sqrt{3}} - 1 \right) \approx -0.00154, \quad (3.9)$$

Moreover, in the limit $\bar{c}_6 \rightarrow 0$, a linear expansion of eq. (3.7) for ZH would lead to the result in ref. [31]. As explained in ref. [36] for hadronic processes, C_1 parametrises contributions that are process and kinematic dependent.

In Fig. 2, we show σ_{LO} (left plot) and C_1 (right plot) for ZH (red) and WBF (green) production as function of the energy of the collider $\sqrt{\hat{s}}$. As expected, while C_1 strongly depends on $\sqrt{\hat{s}}$ for ZH , it does very mildly for WBF H . In particular, for ZH , when increasing the energy, C_1 decreases at the beginning, then changes its sign around $\sqrt{\hat{s}} = 550$ GeV and remains small. On the other hand, the total cross section for ZH production peaks at around $\sqrt{\hat{s}} = 240$ GeV and decreases as $\sqrt{\hat{s}}$ increases, while the cross section for WBF H production increases with $\sqrt{\hat{s}}$. Thus, while for the range 200 – 500 GeV the ZH production is expected to be more sensitive than WBF on $\bar{c}_6(\kappa_3)$, at higher energies the situation is reversed. The information from collisions at different energies, or even at different colliders, increases the sensitivity on κ_3 , as it has been discussed in ref. [43]. We will show analogous results in sec. 4. We have also looked at the differential distribution for the transverse momentum of the Higgs boson, but we have not seen any strong dependence on C_1 . Hence, for single Higgs production at e^+e^- colliders differential distribution cannot increase the sensitivity on κ_3 , at variance with the case of hadron colliders [36, 37, 40, 41] and of double-Higgs production [57].

The range of validity of this calculation in κ_3 and in turn \bar{c}_6 is mainly dictated by the effects from δZ_H^{NP} , as discussed in ref. [36], from which the bound $|\kappa_3| < 20$ can be also straightforwardly applied here. A more cautious and conservative condition can be derived by requiring perturbative unitarity for the $HH \rightarrow HH$ scattering amplitude and/or perturbativity for the loop corrections to the HHH vertex in any kinematic configuration. This bound has been derived in ref. [56] and leads to the requirement $|\kappa_3| < 6$, independently from the value of κ_4 . However, the kinematic configuration leading to this bounds are those involving two Higgses on-shell and the virtuality of the third Higgs close to $2m_H$, which is not relevant for the trilinear interaction entering in single-Higgs production. We independently re-investigated this bound on \bar{c}_6 (and analogous ones on \bar{c}_8) in Appendix C, where its derivation is discussed in detail.

3.2 Double Higgs production

We now consider double Higgs production. The cross sections for the production of two Higgs bosons in association with a Z bosons ($e^+e^- \rightarrow ZHH$) and via WBF ($e^+e^- \rightarrow \nu_e \bar{\nu}_e HH$) do depend on the trilinear Higgs self-coupling already at the tree level (see diagrams in Fig. 3). Moreover, for both processes, one-loop corrections depend on both the trilinear and quartic Higgs self-couplings. At leading order ZHH and WBF HH cross sections can be written as ⁶:

$$\sigma_{\text{LO}}(HH) = \sigma_0 + \sigma_1 \bar{c}_6 + \sigma_2 \bar{c}_6^2, \quad (3.10)$$

⁶The σ_i terms entering eq. (3.10) are not the same quantities appearing in eq. (3.5).

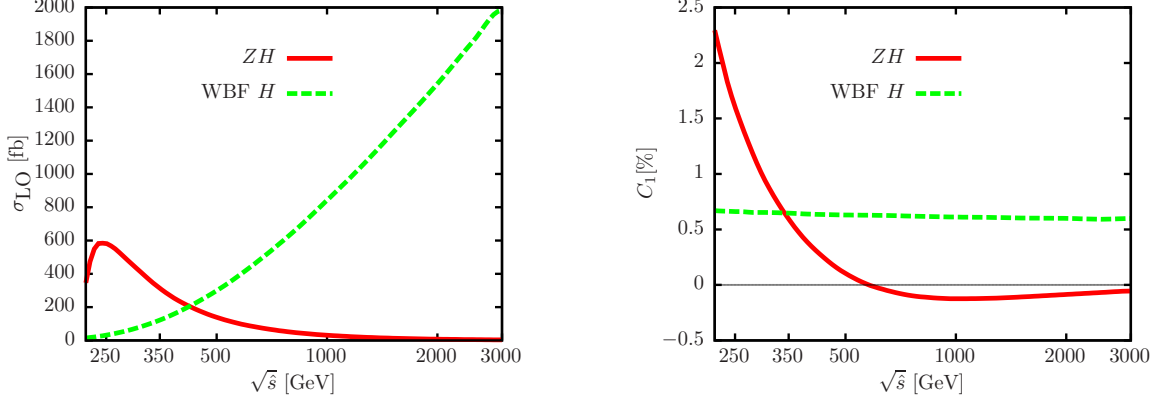


Figure 2: LO cross section (left) and C_1 (right) as function of the center of mass energy \sqrt{s} for $P(e^-, e^+) = (-1.0, 1.0)$.

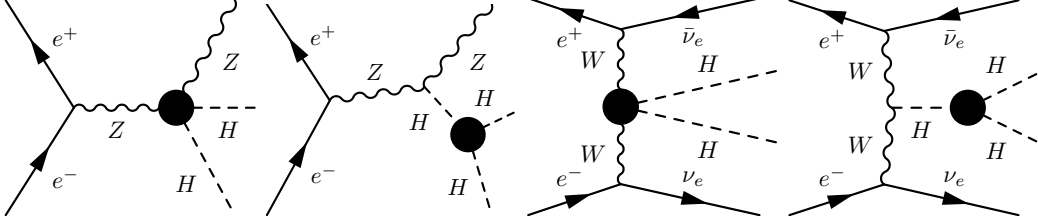


Figure 3: Representative Feynman diagrams for double Higgs production. The black blobs correspond to the one-loop $HHVV$ and HHH form factors.

where σ_0 is the SM result, σ_1 represents the leading contribution in the EFT expansion (order $(v/\Lambda)^2$), while σ_2 is the squared EFT term of order $(v/\Lambda)^4$. Note that within our choice of operators there is no contribution proportional to \bar{c}_8 in this expansion. Actually, no c_{2n} coefficient with $n > 3$ enters at the tree level.

The NLO corrections involve several different contributions. First we classify all of them and then we specify those relevant for our study. Using a notation that is analogous to eq. (3.10), the cross section at NLO accuracy can be parametrised as

$$\sigma_{\text{NLO}}(HH) = \sigma_{\text{LO}}(HH) + \sigma_{1\text{-loop}}(HH) , \quad (3.11)$$

$$\sigma_{1\text{-loop}}(HH) = \sigma_{00} + \sigma_{10}\bar{c}_6 + \sigma_{20}\bar{c}_6^2 \quad (3.12)$$

$$+ \sigma_{30}\bar{c}_6^3 + \sigma_{40}\bar{c}_6^4 \quad (3.13)$$

$$+ \bar{c}_8 \left[\sigma_{01} + \sigma_{11}\bar{c}_6 + \sigma_{21}\bar{c}_6^2 \right] \quad (3.14)$$

$$+ \bar{c}_{10} \left[\sigma_{001} + \sigma_{101}\bar{c}_6 \right] , \quad (3.15)$$

where the σ_{ij} quantities refer to the one-loop terms that factorise $\bar{c}_6^i \bar{c}_8^j$ contributions and the σ_{i0j} to those proportional to $\bar{c}_6^i \bar{c}_{10}^j$. Some comments on the terms in (3.12), (3.13), (3.14) and (3.15) are in order.

The terms in (3.12) are the NLO EW corrections to the contributions that appear already at LO. The quantity σ_{00} , for instance, corresponds to the NLO EW corrections in the SM and has been calculated in ref. [58]. The terms σ_{10} and σ_{20} are $\mathcal{O}(\alpha)$ corrections to σ_1 and σ_2 , respectively, and thus they are always subdominant. They should be included for precise determination of \bar{c}_6 values, yet being subdominant, we neglect them together with σ_{00} in this first analysis, similarly to the case of single Higgs production.

The terms in (3.13) collect contributions that appear at NLO for the first time. For small values $\bar{c}_6 \ll 1$, these terms are suppressed w.r.t. σ_1 and σ_2 in (3.10), and may be neglected. However, at variance with σ_{10} and σ_{20} , for large values of \bar{c}_6 , they are not subdominant. Thus, we keep them in order to study the \bar{c}_6 and in turn κ_3 dependence beyond the linear approximation, which as explained is not sufficient for large values of \bar{c}_6 . Moreover, this allows also to better quantify the range of validity of our perturbative calculation (see Appendix C). These contributions originate from the left diagram of Fig. 4, which shows also the other possible one-loop corrections to the HHH vertex. This diagram induces a $(\bar{c}_6)^3$ dependence in the amplitude and in turn a $(\bar{c}_6)^4$ dependence in $\sigma_{1\text{-loop}}(HH)$ via the interference with Born diagrams. As it has been discussed in ref. [56], its contribution can be large. Also, the presence of $(\bar{c}_6)^3$ effects indicates that terms up to the order $(v/\Lambda)^6$ have to be taken into account in the one-loop amplitudes and thus in the renormalisation constants. Schematically, each order in the (v/Λ) expansion implies that the following terms can be in principle present

$$(v/\Lambda)^2 \rightarrow \{\bar{c}_6\} \rightarrow \{(\lambda_3 - \lambda_3^{\text{SM}})\}, \quad (3.16)$$

$$(v/\Lambda)^4 \rightarrow \{(\bar{c}_6)^2, \bar{c}_8\} \rightarrow \{(\lambda_3 - \lambda_3^{\text{SM}})^2, (\lambda_4 - \lambda_4^{\text{SM}})\}, \quad (3.17)$$

$$(v/\Lambda)^6 \rightarrow \{(\bar{c}_6)^3, \bar{c}_8\bar{c}_6, \bar{c}_{10}\} \rightarrow \{(\lambda_3 - \lambda_3^{\text{SM}})^3, (\lambda_4 - \lambda_4^{\text{SM}})(\lambda_3 - \lambda_3^{\text{SM}}), \lambda_5\}. \quad (3.18)$$

Thus, the full dependence on λ_3 and λ_4 of the diagrams appearing in Fig. 4 is taken into account.⁷ On the other hand, $(v/\Lambda)^6$ terms include c_{10} contributions, which we reparametrised in term of $\bar{c}_{10} \equiv (c_{10}v^6)/(\lambda\Lambda^6)$; they lead to an independent value also for λ_5 , the factor in front of the H^5/v term appearing in $V^{\text{NP}}(\Phi)$ after EWSB. The origin of the terms in (3.14) and (3.15) can be now understood on the base of Fig. 4 and eqs. (3.16)-(3.18) and are commented in the following. The terms in (3.14) are the contributions that depend on \bar{c}_8 . Thus, σ_{01} , σ_{11} and σ_{21} are the most relevant quantities in our one-loop study of double Higgs production, as they provide the sensitivity to \bar{c}_8 and therefore to the deviation from the quadrilinear that one expects on top of the one determined by \bar{c}_6 only. Although σ_{11} and σ_{21} would be suppressed for small c_6 we keep them to study the validity of our calculation in the (\bar{c}_6, \bar{c}_8) plane, or equivalently (κ_3, κ_4) plane.

Finally, the last term (3.15), is related to \bar{c}_{10} -dependent contributions. These contributions arise from the diagram with the H^5 interactions in Fig. 4 and the corresponding term in the renormalisation constant δc_6 (see eq. (A.16) for the explicit δc_6 formula), and

⁷This classification is general enough to include also the effects present at one loop in the $HHVV$ and HVV vertexes, as can be seen in Appendix B.

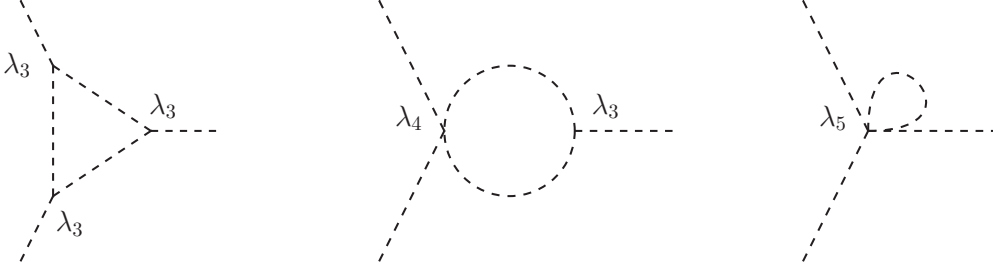


Figure 4: Feynman Diagrams contributing to the HHH form factor at one loop.

can be expressed as

$$\bar{c}_{10} \left[\sigma_{001} + \sigma_{101} \bar{c}_6 \right] = (\sigma_1 + 2\sigma_2 \bar{c}_6) \frac{5\lambda \bar{c}_{10}}{4\pi^2} \left(1 - \log \frac{m_H^2}{\mu_r^2} \right). \quad (3.19)$$

At one-loop in ZHH or WBF production their sum can be written as a kinematically independent shift to \bar{c}_6 ,

$$\bar{c}_6 \rightarrow \bar{c}_6 + \frac{5\lambda \bar{c}_{10}}{4\pi^2} \left(1 - \log \frac{m_H^2}{\mu_r^2} \right) \sim \bar{c}_6 + 0.016 \bar{c}_{10} \left(1 - \log \frac{m_H^2}{\mu_r^2} \right). \quad (3.20)$$

In practice we can only constrain a linear combination of \bar{c}_6 and \bar{c}_{10} that is in eq. (3.20). In the following we work in the assumptions that \bar{c}_{10} effects are negligible and we set $\bar{c}_{10} = 0$, however, for not too large values of \bar{c}_{10} , *i.e.*, where the linear expansion in \bar{c}_{10} is reliable, results of \bar{c}_6 can be translated into a linear combination of \bar{c}_6 and \bar{c}_{10} via eq. (3.20).⁸ In order to be directly sensitive to \bar{c}_{10} one would need to consider one-loop effects in triple Higgs production, or evaluate quadruple Higgs production at the tree level.

In conclusion, in our phenomenological analysis, we evaluate \bar{c}_6 and \bar{c}_8 effects at one loop via the following approximation

$$\begin{aligned} \sigma_{\text{NLO}}^{\text{pheno}}(HH) &= \sigma_{\text{LO}}(HH) + \Delta\sigma_{\bar{c}_6}(HH) + \Delta\sigma_{\bar{c}_8}(HH), \\ \Delta\sigma_{\bar{c}_6}(HH) &= \bar{c}_6^3 \left[\sigma_{30} + \sigma_{40} \bar{c}_6 \right], \\ \Delta\sigma_{\bar{c}_8}(HH) &= \bar{c}_8 \left[\sigma_{01} + \sigma_{11} \bar{c}_6 + \sigma_{21} \bar{c}_6^2 \right]. \end{aligned} \quad (3.21)$$

The analytical results for the form factors used for the calculation of $\Delta\sigma_{\bar{c}_6}(HH)$ and $\Delta\sigma_{\bar{c}_8}(HH)$ are given in Appendix B. We show now the impact of \bar{c}_6 and \bar{c}_8 in the $\sigma_{\text{NLO}}^{\text{pheno}}$ predictions at different energies.

First of all, in Fig. 5 we show the LO cross section σ_{LO} of ZHH (left) and WBF (right) production as function of $\sqrt{\hat{s}}$ for different values of \bar{c}_6 . In ZHH production, the LO cross section peaks around $\sqrt{\hat{s}} = 500$ GeV, which is the optimal energy for measuring this

⁸If \bar{c}_{10} is so large that the shift induced by eq. (3.20) is even larger than \bar{c}_6 itself, then squared loop-diagrams involving the H^5 vertex would be larger than their interferences with Born diagrams. Thus, one-loop contributions, and consequently the level of accuracy of our calculation, would not be sufficient.

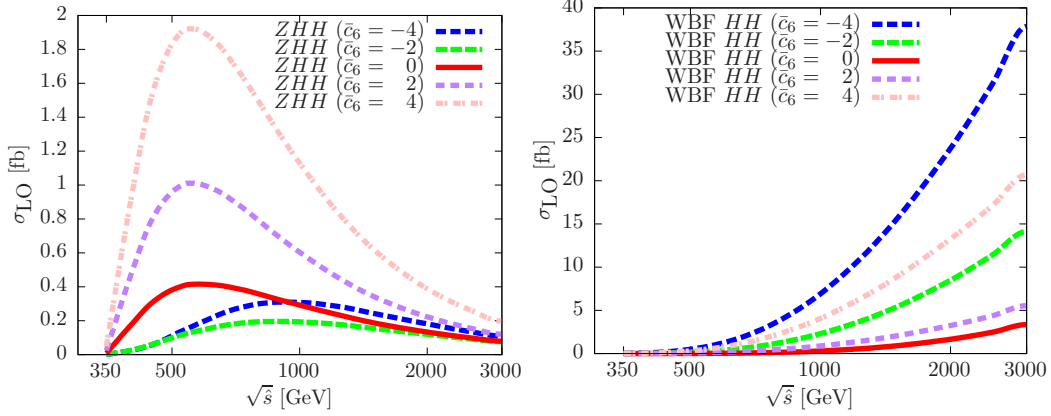


Figure 5: LO cross section of ZHH and WBF HH as function of \sqrt{s} for different values of \bar{c}_6 . Results refer to $P(e^-, e^+) = (-1.0, 1.0)$.

processes, while WBF HH cross section grows with energy. As can be seen by comparing the left and right plot, the dependence on \bar{c}_6 is different in ZHH and WBF HH production. Especially, at variance with ZHH , WBF HH cross sections in general increase when $\bar{c}_6 \neq 0$. This feature is even more clear in the top-left plot of Fig. 6, where we show the dependence of σ_{LO} on \bar{c}_6 for the different phenomenologically relevant configurations that will be analysed in sec. 4, namely, ZHH at 500 GeV collisions and WBF HH at 1, 1.4 and 3 TeV collisions.

Using a similar layout, in Fig. 6 we display three other plots, which show the dependence of σ_{LO} , $\Delta\sigma_{\bar{c}_6}(HH)$ and $\Delta\sigma_{\bar{c}_8}(HH)/\bar{c}_8$ on \bar{c}_6 for different processes and energies. Specifically, in the upper-right plot we show the case of ZHH at 500 GeV, while in the lower plots we show WBF HH at 1 TeV (left) and 3 TeV (right). In these three plots we display σ_{LO} , which has also been shown in the top-left plot, as a black line and $\Delta\sigma_{\bar{c}_6}(HH)$ and $\Delta\sigma_{\bar{c}_8}(HH)/\bar{c}_8$ as a blue and red line, respectively. Thus the blue line directly shows the \bar{c}_8 -independent part of $\sigma_{\text{NLO}}^{\text{pheno}}$, while the red one corresponds to the coefficient in front of the \bar{c}_8 -dependent part $\Delta\sigma_{\bar{c}_8}(HH)$, which in turn depends on \bar{c}_6 . For both cases, a short-dashed line is used when $\Delta\sigma_{\bar{c}_6}(HH)$ or $\Delta\sigma_{\bar{c}_8}(HH)/\bar{c}_8$ are negative. From Fig. 6 we can see that not only for the LO prediction (top-left plot) but also for one-loop effects the \bar{c}_6 (as well \bar{c}_8) dependence is very different in ZHH (top-right plot) and WBF HH (lower plots) production. On the other hand, as can be seen in the lower plots, besides a global rescaling factor, WBF HH results are not strongly affected by the energy of e^+e^- collisions.⁹ In the case of ZHH production at 500 GeV, the minimum of the LO cross section is at $\bar{c}_6 \sim -3$, while for WBF HH it is at $\bar{c}_6 \sim 0.5$. This minimum is given by cancellations induced by the interference of diagrams featuring or not the HHH vertex. Such pattern of cancellations is different in the $\Delta\sigma_{\bar{c}_6}(HH)$ one-loop contribution, which in absolute value is instead minimal at $\bar{c}_6 = 0$ and very large at large values of \bar{c}_6 . For this reason, *e.g.*, for

⁹In the case of ZHH there are larger differences with the energy, but in our analysis we consider it only at 500 GeV.

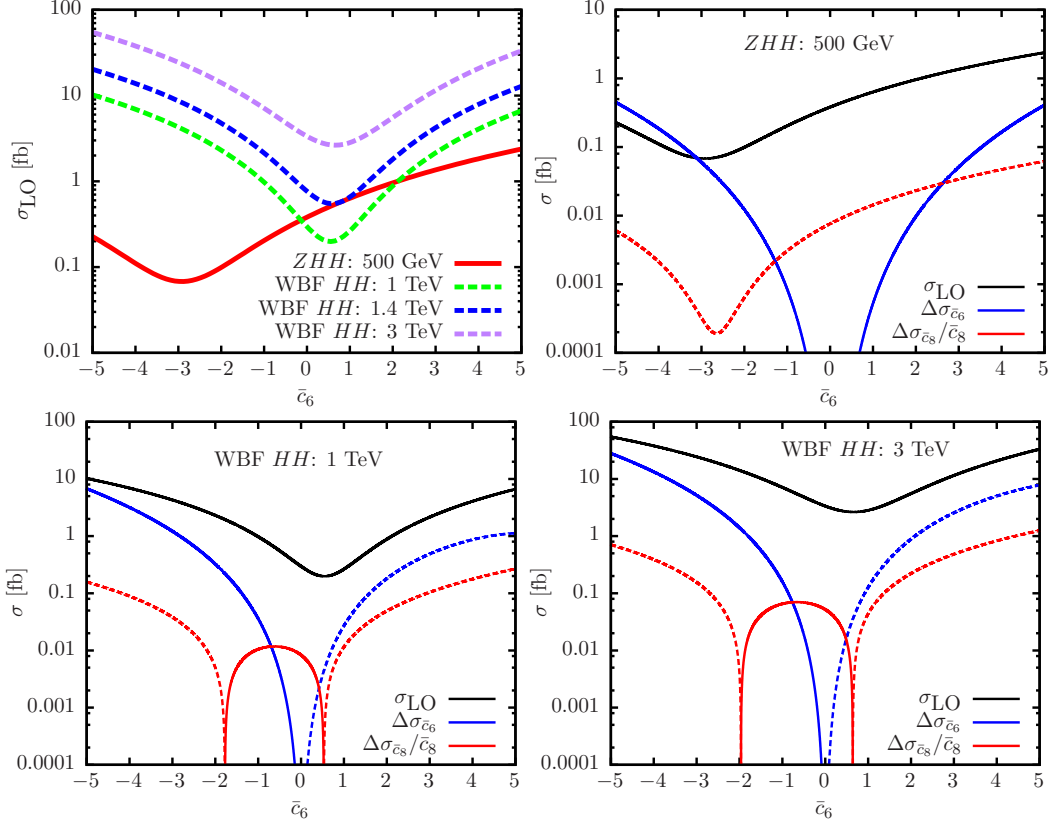


Figure 6: Top-left plot: \bar{c}_6 dependence of the LO cross section for ZHH and $WBF\ HH$ at different energies. The three other plots show the \bar{c}_6 dependence of $\Delta\sigma_{\bar{c}_6}(HH)$, $\Delta\sigma_{\bar{c}_8}(HH)/\bar{c}_8$ and again σ_{LO} for ZHH production at 500 GeV (top-right), and $WBF\ HH$ at 1000 GeV (bottom-left) and 3000 GeV (bottom-right). Negative values are displayed as short-dashed lines.

$\bar{c}_6 < -3$ the $\Delta\sigma_{\bar{c}_6}(HH)$ one-loop contribution is larger than the LO cross section. This does not signal the breaking of the perturbative convergence, rather it is due to the large cancellations that are present in this region only in the LO cross section; as already said, the perturbative limits, which are derived in Appendix C, require $|\bar{c}_6| < 5$ and correspond to the range of the plot. In the case of $WBF\ HH$ production $\Delta\sigma_{\bar{c}_6}(HH)$ is always smaller than σ_{LO} , being negative for $\bar{c}_6 > 0$ and positive for $\bar{c}_6 < 0$.

Regarding the $\Delta\sigma_{\bar{c}_8}(HH)$ contribution, which we display in the red lines normalised with $1/\bar{c}_8$, the effect is very different in ZHH and $WBF\ HH$ production. In the case of ZHH production $\Delta\sigma_{\bar{c}_8}(HH)$ is always negative and the minimum in absolute value is very close to the minimum of the LO prediction. In the case of $WBF\ HH$ production $\Delta\sigma_{\bar{c}_8}(HH)$ change sign at $\bar{c}_6 \sim -2$ and $\bar{c}_6 \sim 0.5$, being positive between these two values and negative outside them. In general, in absolute value, the ratio $\Delta\sigma_{\bar{c}_8}(HH)/\sigma_{\text{LO}}$ is always below $\bar{c}_8 \cdot 2\%$ value. Still, given the allowed perturbative range $|\bar{c}_8| < 31$ (see Appendix C), effects from large values of \bar{c}_8 can be in principle probed.

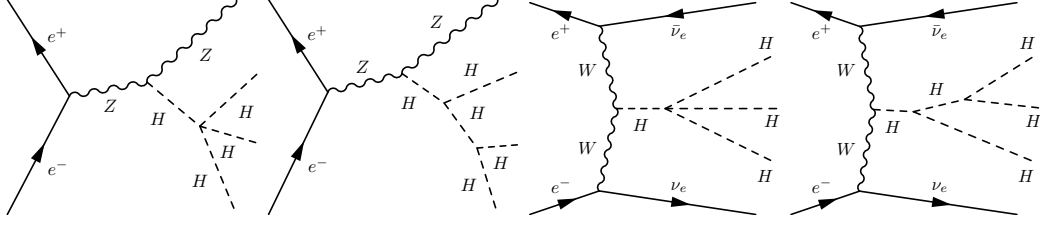


Figure 7: Representative tree-level Feynman diagrams for triple Higgs production.

ratio over σ_{00}	σ_{10}	σ_{20}	σ_{30}	σ_{40}
500 GeV	(2.2, -9.0)	(1.4, 8.5)	(0.3, 34)	(0.02, 19)
1 TeV	(2.2, -3.7)	(1.5, 16)	(0.2, 17)	(0.01, 6)
1.4 TeV	(2.2, -3.4)	(1.6, 16)	(0.2, 12)	(0.01, 3.8)
3 TeV	(2.2, -2.1)	(1.9, 7.6)	(0.2, 3.8)	(0.01, 1.0)
ratio over σ_{00}	σ_{01}	σ_{11}	σ_{21}	σ_{02}
500 GeV	(0.1, -4.0)	(0.1, -14)	(0.01, 16)	(0.002, 3.3)
1 TeV	(0.1, -1.5)	(0.2, 10)	(0.02, 7.1)	(0.006, 2.3)
1.4 TeV	(0.1, -1.0)	(0.2, 9.2)	(0.02, 5.2)	(0.009, 2.0)
3 TeV	(0.1, -0.3)	(0.3, 4.1)	(0.03, 1.6)	(0.02, 0.9)

Table 2: σ_{ij}/σ_{00} ratios for $(ZH\bar{H}H, \text{WBF } H\bar{H}H)$. σ_{ij} are defined in eq. (3.22).

3.3 Triple Higgs production

In triple Higgs production cubic and quartic self-couplings are present already at the tree-level and therefore both the leading dependences on \bar{c}_6 and \bar{c}_8 are already present at LO (see diagrams in Fig. 7). Following the same notation used for double Higgs production, the cross section used for our phenomenological predictions can be written as

$$\sigma_{\text{LO}}(HHH) = \sigma_{00} + \sum_{1 \leq i+2j \leq 4} \sigma_{ij} \bar{c}_6^i \bar{c}_8^j, \quad (3.22)$$

where the σ_{00} term corresponds to the LO SM prediction. Similarly to the case of double Higgs production at one loop, terms up to the eighth power in the (v/Λ) expansion are present at the cross section level, although in this case only the fourth power is present at the amplitude level. The upper bounds on \bar{c}_6 and \bar{c}_8 mentioned in the previous section and discussed in Appendix C have to be considered also in this case. It is important to note that although for large values of \bar{c}_6 and \bar{c}_8 loop corrections may be sizeable, at variance with double Higgs production, \bar{c}_6 and \bar{c}_8 are both entering at LO. Thus, when limits on \bar{c}_6 and \bar{c}_8 are extracted, loop corrections may slightly affect them, but only for large \bar{c}_6 and \bar{c}_8 values. In Tab. 2 we give all the σ_{ij}/σ_{00} ratios, so that the size of all the relative effects from the different NP contributions can be easily inferred.¹⁰ In Fig. 8, we show σ_{LO} at different energies for representative values of \bar{c}_6 and \bar{c}_8 , including the SM case ($\bar{c}_6 = 0, \bar{c}_8 = 0$) where $\sigma_{\text{LO}} = \sigma_{00}$. There, we also explicitly show the value of the σ_{02} component, which factorises

¹⁰There are large cancellations among the different contributions; more digits than those shown here have to be taken into account in order to obtain a reliable result.

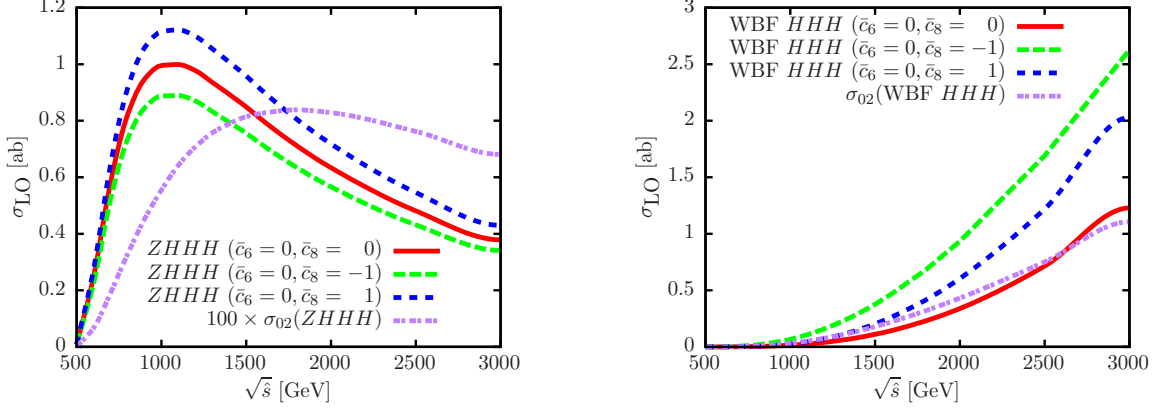


Figure 8: LO cross section of $ZHHH$ and $WBF\ HHH$ as function of \sqrt{s} for representative values of \bar{c}_6 and \bar{c}_8 . The σ_{02} component is also explicitly shown. Results refer to $P(e^-, e^+) = (-1.0, 1.0)$.

the $(\bar{c}_8)^2$ dependence. We can see that for $ZHHH$ production (left) the sensitivity to \bar{c}_8 is rather weak. The σ_{02} component is just around 1% of σ_{00} , which means that even for large values of \bar{c}_8 the total cross section would not be large enough to be measurable at the future colliders considered in this study (see discussion in sec. 4). On the other hand, the total cross section of $WBF\ HHH$ increases with the energy, as for single and double Higgs production. Especially, the σ_{02} component is much larger; it is of the same order of the SM σ_{00} component. As an example, assuming $\bar{c}_8 = 1$ ($\bar{c}_8 = -1$) and $\bar{c}_6 = 0$, σ_{LO} at 3 TeV is 1.7 (2.2) times larger than σ_{00} . For large \bar{c}_8 values, $\sigma_{LO} \approx \bar{c}_8^2 \sigma_{02} \approx \bar{c}_8^2 \sigma_{00}$. As can be seen in Tab. 2, WBF is also very sensitive on \bar{c}_6 ; for large values of \bar{c}_6 indeed $\sigma_{LO} \approx \bar{c}_6^4 \sigma_{40}$ and in particular $\bar{c}_6^4 \sigma_{40} \approx \bar{c}_6^4 \sigma_{00}$ at 3 TeV. All these effects are even larger at lower energies.

4 Bounds on the Higgs self-couplings

In this section we study how the \bar{c}_6 and \bar{c}_8 parameters can be constrained at future lepton colliders via the analysis of single, double, and triple Higgs production. We consider four future e^+e^- colliders, CEPC [45], FCC-ee [46], ILC [47], and CLIC [48, 49], with different operations modes¹¹ that are summarised in Tab. 3. In the following, we will refer to the different scenarios as “collider- \sqrt{s} ” like, *e.g.*, CLIC-3000. Although higher integrated luminosities can be attained at the CEPC and FCC-ee, energies as high as at the ILC and CLIC cannot be reached, since they are circular colliders. As a result, only single Higgs production can be measured at the CEPC and FCC-ee, and therefore only indirect constraints via loop corrections can be set on \bar{c}_6 . Instead, at the ILC and CLIC double Higgs production can be measured. With this process, both \bar{c}_6 and \bar{c}_8 can be constrained, the former via the direct dependence at the Born level and the latter via the indirect dependence

¹¹At the ILC also an operation mode at $\sqrt{s} \sim 350$ GeV is expected, but studies mainly focused on the scan of the $t\bar{t}$ production threshold, ignoring Higgs physics. At CLIC also a slightly different scenario at 380 GeV instead of 350 GeV may be possible.

	\sqrt{s} [GeV]	$P(e^-, e^+)$	Luminosity [ab^{-1}]	Relevant final states
CEPC	250	(0.0,0.0)	5.0	ZH , WBF H
FCC-ee	240	(0.0,0.0)	10.0	ZH , WBF H
	350	(0.0,0.0)	2.6	ZH , WBF H
ILC	250	(-0.8,0.3)	2.0	ZH , WBF H
	500	(-0.8,0.3)	4.0	ZHH , WBF H
	1000	(-0.8,0.2)	2.0	$ZHHH$, WBF $H(H(H))$
CLIC	350	(-0.8,0.0)	0.5	ZH , WBF H
	1400	(-0.8,0.0)	1.5	$ZHHH$, WBF $H(H(H))$
	3000	(-0.8,0.0)	2.0	WBF $H(H(H))$

Table 3: The different operation modes for e^+e^- colliders considered in this work.

through loop corrections. Moreover, even triple Higgs production is kinematically allowed at the ILC and CLIC, allowing to set direct constraints on \bar{c}_8 .

In our analysis we consider the following two scenarios¹²:

1. As expected from a well-behaving EFT expansion, the contribution from \bar{c}_8 is suppressed and we can safely set $\bar{c}_8 = 0$. We explore how well we can measure \bar{c}_6 , not only assuming $\bar{c}_6 \sim 0$, *i.e.*, an SM-like configuration, but also allowing for large BSM effects via $\bar{c}_6 \neq 0$.
2. The value of \bar{c}_8 can be different from zero and leads to non-negligible effects. We explore how well we can constrain \bar{c}_8 and how much \bar{c}_8 can affect the measurement of \bar{c}_6 .

First, we study the sensitivity of ZH^n and WBF processes at the various colliders considered. Then we show combined results for the ILC and CLIC. It is important to note, however, that single Higgs production depends on \bar{c}_8 only via two-loop effects, which we did not calculate in this work (see Tab. 1). Thus, we cannot directly combine single Higgs with double Higgs and triple Higgs in the case of Scenario 2. Nevertheless, we discuss the limit that can be obtained in single Higgs production under the assumption that the \bar{c}_8 -dependent two-loop effects are negligible.

4.1 Single Higgs production

In this section we discuss the constraints that can be obtained on \bar{c}_6 via the single-Higgs production modes. As said, since the effects of \bar{c}_8 are unknown, we restrict our study to the case where it can be ignored, *i.e.*, Scenario 1. We start by considering the case in which we assume that the Higgs potential is like in the SM ($\bar{c}_6 = 0$) and then we consider the BSM case with $\bar{c}_6 \neq 0$.

¹²One may be tempted to explore the regime $\bar{c}_6 = 0$ and $\bar{c}_8 \neq 0$, too. However, this condition is neither motivated by an EFT expansion nor protected by any symmetry. As can be seen from eq. (A.16), a large \bar{c}_8 automatically generates a \bar{c}_6 component via loop corrections.

	\sqrt{s} [GeV]	process	ϵ [%]	C_1 [%]	$\bar{c}_6(\pm 1\sigma)$	$\bar{c}_6(\pm 2\sigma)$
CEPC	250	ZH	0.51	1.6	$(-0.38, 0.42) \cup (8.0, 8.8)$	$(-0.73, 0.88) \cup (7.5, 9.1)$
FCC-ee	240	ZH	0.4	1.8	$(-0.26, 0.28) \cup (9.4, 9.9)$	$(-0.51, 0.57) \cup (9.1, 10.2)$
	240	WBF H	2.2	0.66	$(-2.81, 5.1)$	$(-4.3, 6.6)$
	350	WBF H	0.6	0.65	$(-1.15, 3.4)$	$(-1.89, 4.1)$
ILC	250	ZH	0.71	1.6	$(-0.52, 0.59) \cup (7.8, 8.9)$	$(-0.98, 1.3) \cup (7.1, 9.4)$
	500	WBF H	0.23	0.63	$(-0.56, 2.7)$	$(-0.97, 3.1)$
	1000	WBF H	0.33	0.61	$(-0.78, 2.7)$	$(-1.3, 3.3)$
CLIC	350	ZH	1.65	0.59	$(-2.48, 4.3)$	$(-3.80, 5.6)$
	1400	WBF H	0.4	0.61	$(-0.91, 2.9)$	$(-1.50, 3.5)$
	3000	WBF H	0.3	0.59	$(-0.75, 2.6)$	$(-1.26, 3.1)$

Table 4: Expected precision ϵ for the measurements of single Higgs production modes and the expected 1σ and 2σ constraints on \bar{c}_6 , assuming an SM measurement, are listed. The value of ϵ for the CEPC has been taken or obtained via a luminosity rescaling from ref. [45], for the FCC-ee from ref. [46], for the ILC from refs. [47, 59] and for the CLIC from ref. [49].

In Tab. 4 we show 1σ and 2σ constraints on \bar{c}_6 that can be obtained via ZH and WBF H at different energies and colliders, using eq. (3.7). We show also the value of C_1 and the accuracy ϵ that can be achieved in any experimental setup, as provided in [45–47, 49, 59] or obtained from them via a luminosity rescaling.¹³ In general in this work, unless differently specified, we assume Gaussian distributions for the errors and no correlations among them, and the errors are rescaled according to cross section in BSM cases. In the results of Tab. 4 we did not take into account effects due to \bar{c}_6 in the Higgs decay, since, at variance with the LHC case, they can be in principle neglected at e^+e^- colliders. Indeed, the total cross section of $e^+e^- \rightarrow ZH$ production can be measured via the recoiling mass method [47], without selecting a particular H decay channel. Using the same method, the branching ratio of any (visible) decay channel can be precisely measured and used as input in the WBF H analysis, so that also in this case effects due to \bar{c}_6 in the Higgs decay can be neglected. Nevertheless, we explicitly checked that taking into account \bar{c}_6 effects in the decay for the $H \rightarrow b\bar{b}$ channel, which will be the one most precisely measured, results in Tab. 4 are almost unchanged.

As can be seen in eq. (3.7), not only a linearly \bar{c}_6 dependent term is present, but also a \bar{c}_6^2 one. Since C_2 is negative and C_1 is positive for both ZH and WBF H , the SM cross section value is degenerate in \bar{c}_6 ; besides the SM case $\bar{c}_6 = 0$ also a second different $\bar{c}_6 \neq 0$ condition is giving the same value of the cross section. While for the WBF H this second solution is close to $\bar{c}_6 = 2$, in ZH at 240-250 GeV this is around $\bar{c}_6 = 9$, depending on the energy. As a result, the two solutions being close to each other, in WBF H the 1σ and 2σ intervals are always broad, while in ZH at 240-250 GeV we see two narrow intervals: one around $\bar{c}_6 = 0$ and one around $\bar{c}_6 = 9$. Note that for CLIC-350 also ZH is yielding a broad interval as a constraint, since ϵ is larger and C_1 is smaller. Via the combined measurement

¹³In the case of WBF H at ILC, *e.g.*, only the $H \rightarrow b\bar{b}$ has been considered for obtaining the value of ϵ . Thus, smaller values of ϵ may be also achieved.

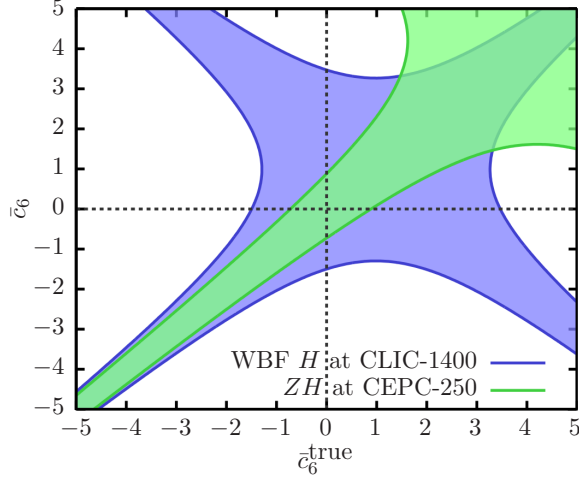


Figure 9: The 2σ bounds on \bar{c}_6 as a function of \bar{c}_6^{true} in single Higgs production in the Scenario 1 described in the text. Two representative cases are considered: ZH at CEPC-250 and WBF H at CLIC-1400.

of ZH and WBF H processes, or including LHC results in a global fit, the \bar{c}_6 region around $\bar{c}_6 = 9$ can be excluded. In conclusion, assuming no other BSM effects, the best constraints on \bar{c}_6 via *single Higgs production* can be obtained at low energy and high luminosity.

We now consider the situation in which \bar{c}_6 has a value different from zero, which will denote as \bar{c}_6^{true} , and we explore the constraints that can be set on \bar{c}_6 , by varying the value of \bar{c}_6^{true} . In Fig. 9 we consider ZH at CEPC-250 and WBF H at CLIC-1400 as examples.¹⁴ The bands in the plot show which constraints on \bar{c}_6 (y-axis) can be set, depending on the value of \bar{c}_6^{true} (x-axis). We considered only the $-5 < \bar{c}_6, \bar{c}_6^{\text{true}} < 5$ range, so that results can be directly compared with the analogous analysis performed in the next section for double Higgs production, where this range cannot be extended without violating perturbativity (see Appendix C). The “X” shapes of the ZH and WBF H bands can be understood as follows. In the limit of zero uncertainties two solutions can be obtained from the equation $\sigma_{\text{NLO}}^{\text{pheno}}(\bar{c}_6) = \sigma_{\text{NLO}}^{\text{pheno}}(\bar{c}_6^{\text{true}})$:

$$\bar{c}_6 = \bar{c}_6^{\text{true}}, \quad (4.1)$$

$$\bar{c}_6 = -\frac{C_1}{\delta Z_H^{\text{SM},\lambda}} - 2 - \bar{c}_6^{\text{true}}, \quad (4.2)$$

which intersect each other at the point $P = \left(-\frac{C_1}{2\delta Z_H^{\text{SM},\lambda}} - 1, -\frac{C_1}{2\delta Z_H^{\text{SM},\lambda}} - 1\right)$. For ZH at CEPC-250 $P = (4.2, 4.2)$ and for WBF H at CLIC-1400 $P = (1.0, 1.0)$.¹⁵ The uncertainties ϵ , however, are not negligible and determine the width of the branches, which are centred on the solutions in eqs. (4.1) and (4.2).

For ZH production, due to the large value of C_1 , only one branch is present in the $-5 < \bar{c}_6, \bar{c}_6^{\text{true}} < 5$ region. Instead, for WBF H , since C_1 is small, SM-like scenarios $\bar{c}_6^{\text{true}} \sim 0$

¹⁴The case of CLIC-350 can be directly seen in Fig. 14, which is described later in the text. In this case, since the value of ϵ is larger, weaker constraints can be set w.r.t. CEPC-250.

¹⁵If we consider ZH at FCC-ee-240 we obtain $P = (4.9, 4.9)$.

	$\sqrt{\hat{s}}$ [GeV]	process	ϵ
ILC [60]	500	ZHH	19%
	1000	WBF HH	23%
CLIC [49]	1400	WBF HH	33%
	3000	WBF HH	15%

Table 5: Expected precision ϵ for the measurements of double Higgs production processes. For the ILC the values of ϵ have been obtained rescaling the values in [60] to the luminosity of Tab. 4. In the case of CLIC, we have derived the values of ϵ via the relations in section 9 of ref. [49].

lies in the intersection region of the branches. Thus, as already previously discussed, ZH provides stronger constraints for $\bar{c}_6^{\text{true}} \sim 0$. On the contrary, for $\bar{c}_6^{\text{true}} \sim 4$, WBF H constraints are stronger. We remind the reader that it is not obvious that the LHC, even after accumulating 3000 fb^{-1} of luminosity, will be able to exclude a value $\bar{c}_6 \sim 4$. Still, with a single measurement for $\bar{c}_6^{\text{true}} \sim 4$ both the intervals around $\bar{c}_6 \sim 4$ and $\bar{c}_6 \sim -3$ are allowed, but the latter may be probed also at the LHC. As shown in Tab. 4, also for ZH and $\bar{c}_6^{\text{true}} \sim 0$ there is a second interval in the constraints, but it is outside the range of the plot.

4.2 Double Higgs production

We now turn to the case of double Higgs production. The expected precisions ϵ for the measurements considered in our analysis¹⁶ are listed in Tab. 5. Although double Higgs production cannot be measured as precise as single Higgs production, it depends on \bar{c}_6 at LO and therefore the sensitivity on this parameter is much higher.

We start our analysis considering Scenario 1, where we set $\bar{c}_8 = 0$. As can be seen in sec. 3.2, the WBF HH dependence on \bar{c}_6 is similar for different energies. For this reason, for Scenario 1, we show WBF HH only for CLIC-1400, together with ZHH at ILC-500. Similarly to Fig. 9, which concerns the case of single Higgs production, in Fig. 10 we plot the constraints that can be set on \bar{c}_6 , by varying the value of \bar{c}_6^{true} . Also in $\sigma_{\text{LO}}(HH)$ both a linear and quadratic dependence on \bar{c}_6 are present, leading to “X”-shape bands. The “X”-shape is slightly asymmetric due to the one-loop σ_{30} and σ_{40} contributions that are present in $\sigma_{\text{NLO}}^{\text{pheno}}(HH)$, see eq. (3.21), which we always use in our study. The central points of the “X” bands are around $(\bar{c}_6^{\text{true}}, \bar{c}_6) = (-2.5, -2.5)$ for ZHH at ILC-500, and around $(\bar{c}_6^{\text{true}}, \bar{c}_6) = (0.5, 0.5)$ for WBF HH at CLIC-1400. For this reason, although the WBF HH band is narrower due to a larger \bar{c}_6 dependence, for values $\bar{c}_6^{\text{true}} \sim 0$, ZHH at ILC-500 is giving better constraints. On the other hand, for values $\bar{c}_6^{\text{true}} \neq 0$ and especially $\bar{c}_6^{\text{true}} \sim -2.5$, WBF HH at CLIC-1400 is leading to better constraints. It is interesting to note that the central points of the “X” bands in WBF H and WBF HH are very close, while for ZH and ZHH they are different. This implies that the combination of the information

¹⁶ Note that the value of ϵ listed in ref. [49, 60] are for a different luminosities than those considered in Tab. 3. Since the statistical uncertainty is the dominant one, the values of ϵ in Tab. 5 have been obtained by rescaling those of ref. [49, 60] proportionally to the square root of the luminosity.

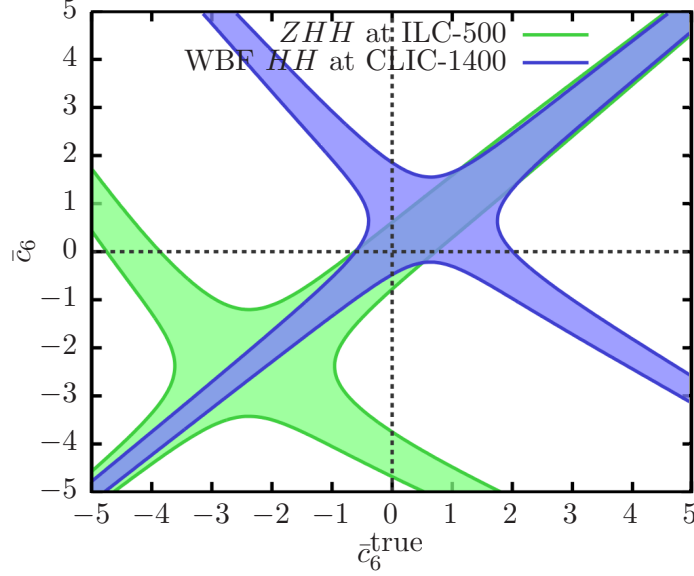


Figure 10: The 2σ bounds on \bar{c}_6 as a function of \bar{c}_6^{true} in double Higgs production in the Scenario 1 described in the text. Two representative cases are considered: ZHH at ILC-500 and WBF HH at CLIC-1400.

from WBF single and double Higgs production would not exclude any of the branches of the “X” shape. Thus, the information from ZH or ZHH is necessary for this purpose. We will comment again this point in sec. 4.4.

We now consider Scenario 2. Specifically, we assume that the true value for \bar{c}_6 is \bar{c}_6^{true} and that the measured cross section for double Higgs production is $\sigma^{\text{measured}} = \sigma_{\text{NLO}}^{\text{pheno}}(\bar{c}_6 = \bar{c}_6^{\text{true}}, \bar{c}_8 = 0)$ and we show which value of (\bar{c}_6, \bar{c}_8) can be constrained via the prediction of $\sigma_{\text{NLO}}^{\text{pheno}}(\bar{c}_6, \bar{c}_8)$. Starting with the SM case, we show results for $\sigma^{\text{measured}} = \sigma_{\text{NLO}}^{\text{pheno}}(\bar{c}_6 = 0, \bar{c}_8 = 0)$ in Fig. 11. We consider the range $|\bar{c}_6| < 5$ and $|\bar{c}_8| < 31$, because as explained in Appendix C for larger values the perturbative calculations cannot be trusted. The plot on the left shows the constraints for ZHH and WBF HH at the ILC-500, while the one on the right those for WBF HH at CLIC-1400 and CLIC-3000. First of all we can notice that the constraints on \bar{c}_6 are weaker than in Scenario 1. Also, no constraints on \bar{c}_8 independently from \bar{c}_6 can be set. On the other hand, the largest part of the (\bar{c}_6, \bar{c}_8) plane can be excluded and the shape of the band depends on the process. It is important to note that this results depend on the choice of the renormalisation scale μ_r and therefore the scale at which $\bar{c}_6(\mu_r)$ and $\bar{c}_8(\mu_r)$ are measured. Our results refers to $\mu_r = 2m_H$, which corresponds to the production threshold for the HH pair and therefore to the phase-space region associated to the bulk of the cross section. While the region close to the SM ($\bar{c}_6 \sim 0, \bar{c}_8 \sim 0$) is very mildly affected by this choice, we warn the reader that the border of the plane $|\bar{c}_6| \sim 5$ and $|\bar{c}_8| \sim 31$ can be strongly affected.

We then consider how the constraints in the (\bar{c}_6, \bar{c}_8) plane depend on the value of σ^{measured} . We consider BSM configurations $\sigma^{\text{measured}} = \sigma_{\text{NLO}}^{\text{pheno}}(\bar{c}_6 = \bar{c}_6^{\text{true}}, \bar{c}_8 = 0)$ with

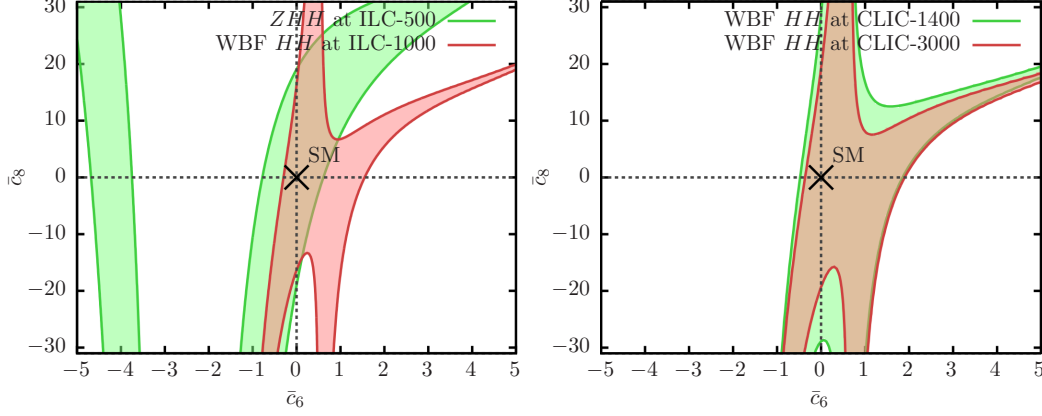


Figure 11: 2σ bounds in the (\bar{c}_6, \bar{c}_8) plane assuming SM cross sections for double Higgs production in the Scenario 2 described in the text. Left: ZHH at ILC-500 and $WBF\ HH$ at ILC-1000. Right: $WBF\ HH$ at CLIC-1400 and CLIC-3000.

$\bar{c}_6^{\text{true}} \neq 0$.¹⁷ In Fig. 12 we show the plots for the values of $\bar{c}_6^{\text{true}} = -4, -2, -1, 1, 2, 4$; in each plot the point $(\bar{c}_6^{\text{true}}, \bar{c}_8^{\text{true}} = 0)$ is displayed with a cross and the value of \bar{c}_6^{true} is given. For these plots, only results for ZHH at ILC-500 and $WBF\ HH$ at ILC-1000 are displayed. Similarly to the SM case, given a value of \bar{c}_6^{true} , the constraints on \bar{c}_6 independent from \bar{c}_8 are weaker than those in Scenario 1. However, also in these cases, the largest part of the (\bar{c}_6, \bar{c}_8) plane can be excluded and the shapes of the bands strongly depend both on the process and the value of \bar{c}_6^{true} . In all cases, ZHH and $WBF\ HH$ sensitivities are complementary; as we will see in sec. 4.4, their combination improves the constraints in the (\bar{c}_6, \bar{c}_8) plane. This is a clear advantage for the ILC, where both ZHH and $WBF\ HH$ can be precisely measured.

The shapes of the green and red bands can be qualitatively explained as follow. Without \bar{c}_8 effects the green and red bands would simply consist of either two separate (narrow) bands or a single large band, consistently with the results that could be obtained by vertically slicing the bands in Fig. 10. The \bar{c}_8 effects bend the bands, leading to the shapes that can be observed in Fig. 12. It is interesting to note that the improvement from CLIC-1400 to CLIC-3000 is rather mild. The main reason is that the increment of the $WBF\ HH$ cross section is compensated by the decrement of its dependence on \bar{c}_6 , which can be directly observed in the top-left plot of Fig. 6.

4.3 Triple Higgs production

We now consider the case of triple Higgs production. In the SM $ZHHH$ and $WBF\ HHH$ production processes have a too small cross section for being observed. As an example, if we consider LR -polarised beams at 1 TeV and the dominant decay into a $b\bar{b}$ pair for the three Higgs bosons and into jets for the Z boson, about 6 ab^{-1} of integrated luminosity would be necessary for one signal event in the SM. As can be seen in Fig. 8, with $WBF\ HHH$ the cross section is even smaller in the SM, on the other hand this process has a strong

¹⁷As the total cross section depends on \bar{c}_8 mildly, we do not expect that the constraints depend on \bar{c}_8^{true}

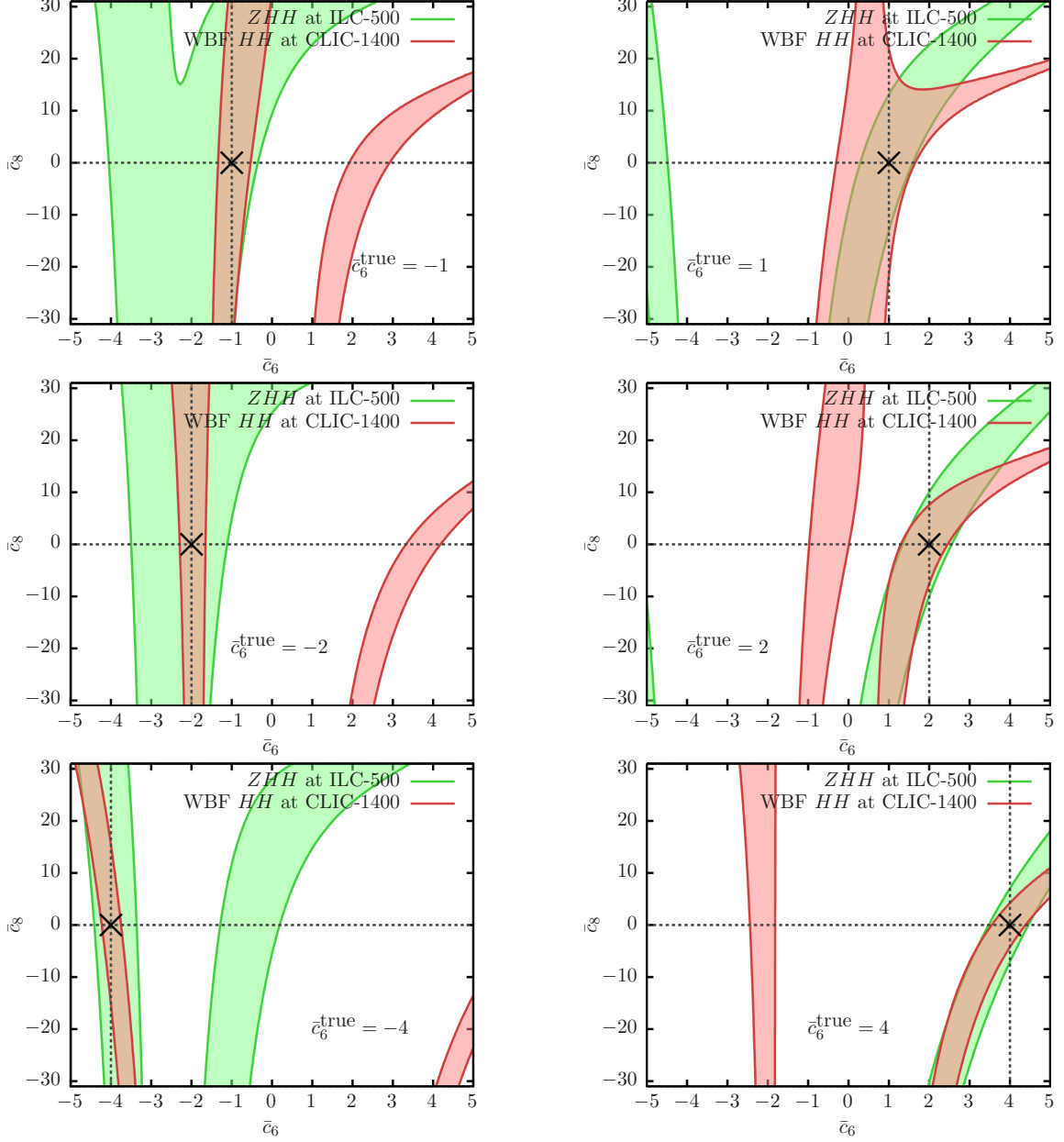


Figure 12: 2σ bounds in the (\bar{c}_6, \bar{c}_8) plane assuming BSM cross sections in double Higgs production corresponding to $(\bar{c}_6^{\text{true}}, \bar{c}_8^{\text{true}} = 0)$ in the Scenario 2 described in the text, with $\bar{c}_6^{\text{true}} = -4, -2, -1, 1, 2, 4$ marked in the plots with a cross. All plots show results for ZHH at ILC-500 and WBF HH at CLIC-1400.

sensitivity on \bar{c}_8 , due to the large value of σ_{02} factorising the \bar{c}_8^2 dependence. Thus, limits on \bar{c}_6 and \bar{c}_8 can be set, but only considering Scenario 2 where \bar{c}_8 can be different from zero.

At variance with double Higgs production, given the very small number of events, we cannot set limits on the (\bar{c}_6, \bar{c}_8) plane by assuming $\sigma^{\text{measured}}(HHH) = \sigma_{\text{LO}}(\bar{c}_6 = \bar{c}_6^{\text{true}}, \bar{c}_8 =$

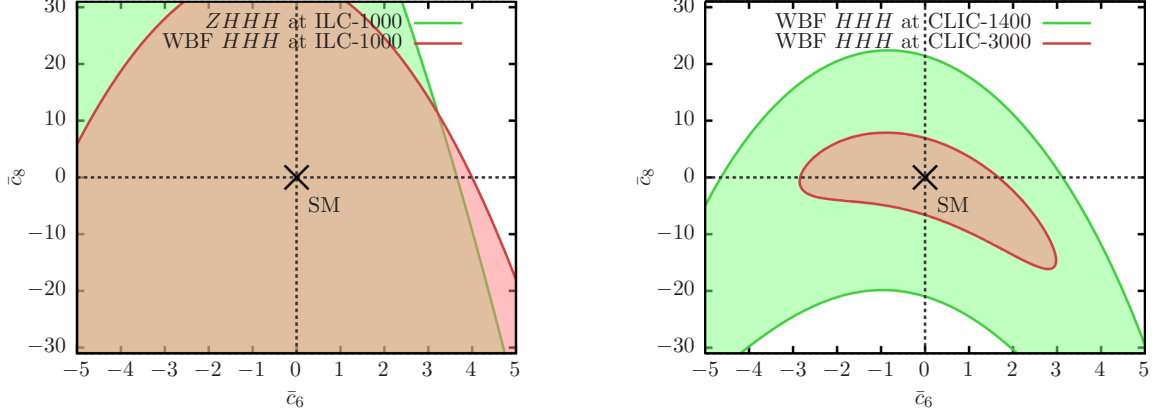


Figure 13: 2σ bounds in the (\bar{c}_6, \bar{c}_8) plane assuming SM cross sections in triple Higgs production in the Scenario 2 described in the text. Left: $ZHHH$ and $WBF HHH$ at ILC-1000. Right: $WBF HHH$ at CLIC-1000 and CLIC-1400.

0). Indeed, the number of events expected is close to zero and a Gaussian fit cannot be performed. Rather, we have to assume events are zero and compare them with the expected value of events for a given $(\bar{c}_6^{\text{true}}, \bar{c}_8^{\text{true}})$ performing a Poissonian analysis.¹⁸ We assume that the other SM backgrounds are giving zero events and we estimate the signal efficiency ε_{HHH} by rescaling the one known for $WBF HH$ production ε_{HH} . In practice, for both $WBF HHH$ and $ZHHH$ production we estimate the signal efficiency to be $\varepsilon_{HHH} = \varepsilon_{HH}^{\frac{3}{2}} = 4.7\%$, where ε_{HH} has been taken from ref. [57].

In Fig. 13, we show the 2σ bounds in the (\bar{c}_6, \bar{c}_8) plane. The plot on the left shows the constraints for $ZHHH$ and $WBF HHH$ at ILC-1000, while the one on the right shows those for $WBF HHH$ at CLIC-1400 and CLIC-3000. As can be seen, at ILC-1000 almost all the (\bar{c}_6, \bar{c}_8) plane is compatible with a zero event condition, both for $ZHHH$ and $WBF HHH$ production. On the other hand, at CLIC-1400 and especially at CLIC-3000 a vast area of the plane can be excluded via the study of $WBF HHH$ production. In particular, at CLIC-3000, the constraint on \bar{c}_8 is comparable to those obtainable at a future 100 TeV hadron collider [28, 29]. The constraints on \bar{c}_6 are instead worse than in the double Higgs production case.

4.4 Combined bounds

We now investigate the constraints that can be obtained via the combination of the information from single, double and triple Higgs production. We consider both Scenarios 1 and 2 and, as already mentioned, in the case of Scenario 2 we combine only results from double and triple Higgs production. We show in parallel the limits on \bar{c}_6 from single Higgs production by assuming that the \bar{c}_8 -dependent two-loop effects are small.

We start discussing the Scenario-1 analysis, separately considering the ILC and CLIC. For both colliders we progressively include results at higher energies in three stages. In

¹⁸In fact, for the case of CLIC-3000, large \bar{c}_6 values would lead to ~ 5 expected events. We will consider this effect in the combined analysis in sec. 4.4.

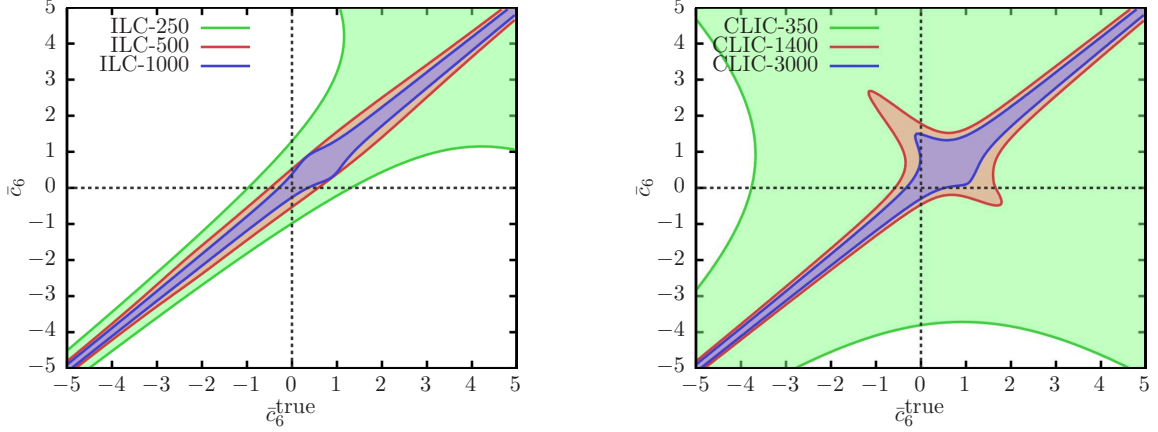


Figure 14: Combined 2σ constraints on \bar{c}_6 as a function of \bar{c}_6^{true} for the ILC (left) and the CLIC (right) in the Scenario 1 described in the text.

the case of the ILC, we start with ZH at ILC-250, in a second step we include ZHH and WBF H results from ILC-500 and finally $ZHHH$ and WBF $H(H(H))$ from ILC-1000. Instead, in the case of the CLIC, we start with ZH at CLIC-350, in a second step we include WBF $H(H(H))$ and $ZHHH$ results from CLIC-1400 and finally WBF $H(H(H))$ results from CLIC-3000. In the case of triple Higgs production we assume that we observe as many events as predicted by $\sigma_{\text{LO}}(HHH)$ in eq. (3.22), with $\bar{c}_8 = 0$.

In Fig. 14, we show the combined results for the ILC (left) and CLIC (right) assuming Scenario 1. In the first stage, both ILC-250 and CLIC-350 constraints are worse than those of CEPC-250 shown in Fig. 9. This is due to a lower precision in the measurements (ϵ) and for CLIC-350 also a smaller value of C_1 . However, in the second stage, including results at higher energies, for both colliders constraints are much stronger, since double Higgs production becomes available. Especially, combining single and double Higgs production the “X” shape disappears and only the band around the line $\bar{c}_6 = \bar{c}_6^{\text{true}}$ remains.¹⁹ In the case of the CLIC, bumps are still present at $\bar{c}_6 \sim 1$, which originate from the centre of the “X”-shape band for WBF $H(H)$ at CLIC-1400, see Fig. 9 and Fig. 10. For the same reason, also for the ILC the band is slightly larger around $\bar{c}_6 \sim 1$. In the third stage, constraints are improved both for the ILC and CLIC. Still, the weaker bounds can be set for $\sim 0 < \bar{c}_6^{\text{true}} < 1$, where the center of the “X”-shape band for WBF HH is located. In this region, constraints are better at the ILC thanks to the ZHH contribution at 500 GeV, which helps to resolve this region.

We now consider Scenario 2. As done in the case of double Higgs production we assume that the true value for \bar{c}_6 is \bar{c}_6^{true} and that $\sigma^{\text{measured}} = \sigma_{\text{NLO}}^{\text{pheno}}(\bar{c}_6 = \bar{c}_6^{\text{true}}, \bar{c}_8^{\text{true}} = 0)$ while that for triple Higgs production we observe as many events as predicted by $\sigma_{\text{LO}}(HHH)$ in eq. (3.22), with $\bar{c}_8 = 0$. In the case of the ILC, we consider ZHH at ILC-500 and its combination with ILC-1000 results from $ZHHH$ and WBF $HH(H)$ production. In the case of CLIC, we consider $ZHHH$ and WBF $HH(H)$ production at CLIC-1400 and its

¹⁹In the case of CLIC, where the ZHH information is not entering the combination, also the information from triple Higgs production is necessary for this purpose.

combination with WBF $HH(H)$ at CLIC-3000. Thus, while ILC-500 is not a combined result, being simply obtained for ZHH production, all the others include information from both double and triple Higgs production. As already said, single Higgs production cannot be directly included in the combination, since its \bar{c}_8 dependence starts at two-loop level.

In Fig. 15 we show results for the SM case ($\bar{c}_6^{\text{true}} = 0, \bar{c}_8^{\text{true}} = 0$) as green bands. There we also show as red bands the limits on \bar{c}_6 extracted from single Higgs measurements at the ILC and CLIC²⁰, assuming that the two-loop \bar{c}_8 dependence is negligible. Due to the available higher energies, combined double and triple Higgs constraints at the CLIC are better than at the ILC. Indeed the WBF $HH(H)$ production cross section increases with the energy. On the other hand, single Higgs production can be better measured at the ILC and therefore the corresponding constraints on \bar{c}_6 are better than at the CLIC. We notice that the only case where single Higgs results may be relevant in a further combination with those from double and triple Higgs production is the case of ILC-500, which is actually coming from only ZHH production. Indeed, the combination of ZH at ILC-250 and WBF H at ILC-500 would help in removing the band around $\bar{c}_6 = -4$, and shrinking the possible region for the band around SM value. On the contrary, at higher energies the WBF HH production is more relevant in constraining \bar{c}_6 . Thus, with the exception of ILC-500, single Higgs production could be helpful in constraining the (\bar{c}_6, \bar{c}_8) plane only if the dependence on \bar{c}_8 at two-loop is larger than what we assumed or if low-energy runs at higher luminosity, such as those at circular colliders, are considered.

In Fig. 16 we show the constraints from the combination of double and triple Higgs for BSM cases $\bar{c}_6^{\text{true}} = -4, -2, -1, 1, 2, 4$. As already discussed for the SM case, constraints from single Higgs production are negligible for high energy e^+e^- colliders in this scenario under our assumptions and for this reason they are not shown. We display in each plot both CLIC and ILC bounds. As we can see, both in the SM and in all BSM cases considered, the combination of results from double and triple Higgs production is always strongly improving the bounds. Also, with higher energies, stronger constraints can be set; the best results can be obtained combining results at CLIC-1400 with those at CLIC-3000, especially for $\bar{c}_6^{\text{true}} \neq 0$ since a non-zero number of events can be observed. It is interesting to note that CLIC bounds around $(\bar{c}_6^{\text{true}}, \bar{c}_8^{\text{true}})$ are less sensitive than at the ILC on the value of \bar{c}_6^{true} , featuring vertical elongated contours in the (\bar{c}_6, \bar{c}_8) plane. The reason is that at CLIC bounds mainly comes from WBF HHH , while at the ILC mainly from double Higgs production, both ZHH and WBF HH .

In conclusion we observed that low- and high-energy runs are useful for constraining the shape of the Higgs potential. Under the assumption of Scenario 1, we have shown the complementarity of ZH production at low energy with WBF HH information at higher energies. Under the Scenario 2, we have shown that the combination of the information from double and triple Higgs production, which is possible only at high energy, improves the constraints in the (\bar{c}_6, \bar{c}_8) plane (*cf.* fig. 12 with fig. 16).

²⁰ More specifically, for the ILC, the single Higgs limit are combined results from ZH at ILC-250, WBF H at ILC-500, and WBF H at ILC-1000, while for the CLIC, the single Higgs limit are combined results from ZH at CLIC-350, WBF H at CLIC-1400, and WBF H at CLIC-3000.

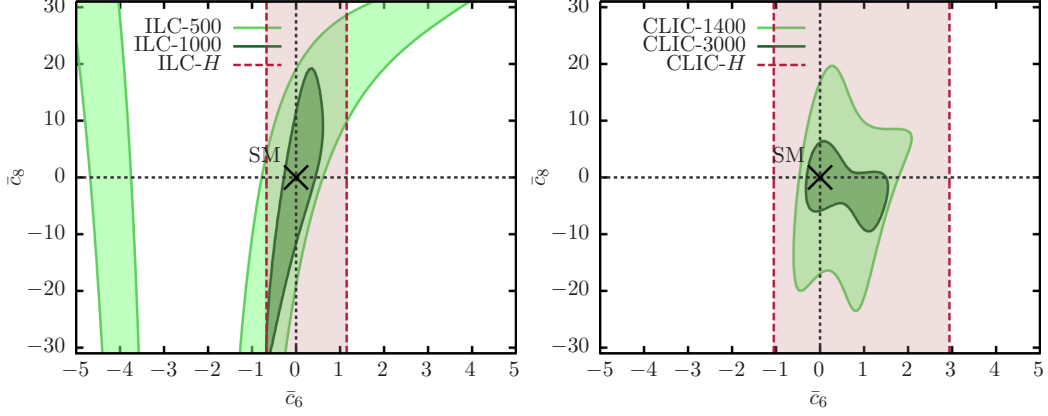


Figure 15: Combined 2σ constraints in the (\bar{c}_6, \bar{c}_8) assuming SM cross sections, at the ILC (left) and CLIC (right), in the Scenario 2 described in the text. ILC- H and CLIC- H refer to a combination of all single Higgs measurements at all energy stages for each collider under study.

5 Conclusions

Determining whether the scalar potential for the Higgs boson is the minimal one predicted by the SM is among the main targets of the current and future colliders. In this work, we have investigated the possibility of setting constraints on the shape of the Higgs potential via the measurements of single, double and triple Higgs production at future e^+e^- colliders, considering the two dominant channels, *i.e.*, Z boson associate production (ZH^n) and W boson fusion WBF. In order to leave the possibility for the trilinear and quadrilinear couplings to vary independently, we have added to the SM potential two EFT operators $\frac{c_6}{\Lambda^2} (\Phi^\dagger \Phi - \frac{1}{2}v^2)^3$ and $\frac{c_8}{\Lambda^4} (\Phi^\dagger \Phi - \frac{1}{2}v^2)^4$ and calculated the tree-level and one-loop dependence on c_6 and c_8 for single and double Higgs production as well as tree-level results for triple Higgs production (see also Tab. 1 in sec.1).

One-loop corrections to single Higgs production, which depends only on λ_3 and thus c_6 , have already been calculated and studied in the literature and we have confirmed previous results. On the other hand, the one-loop dependence on λ_4 and therefore on c_6 and c_8 of double Higgs production has been calculated for the first time here. At variance with the case of single Higgs production, the EFT parametrisation is in this case compulsory and an anomalous coupling approach cannot be consistently used; the c_6 parameter is itself renormalised and receives corrections from both c_6 and c_8 . We have provided all the necessary renormalisation constants and counterterms and expressed the finite one-loop results via analytical form factors that can be directly used in phenomenological applications. We have also motivated the inclusion of the “ $-\frac{1}{2}v^2$ ” term in the EFT parametrisation, which simplifies the renormalisation procedure by preserving the relations among the SM counterterms. Nevertheless, results can always be easily translated to the $\frac{c'_6}{\Lambda^2} (\Phi^\dagger \Phi)^3$ and $\frac{c'_8}{\Lambda^4} (\Phi^\dagger \Phi)^4$ basis.

In our phenomenological analyses we have considered several experimental setups at

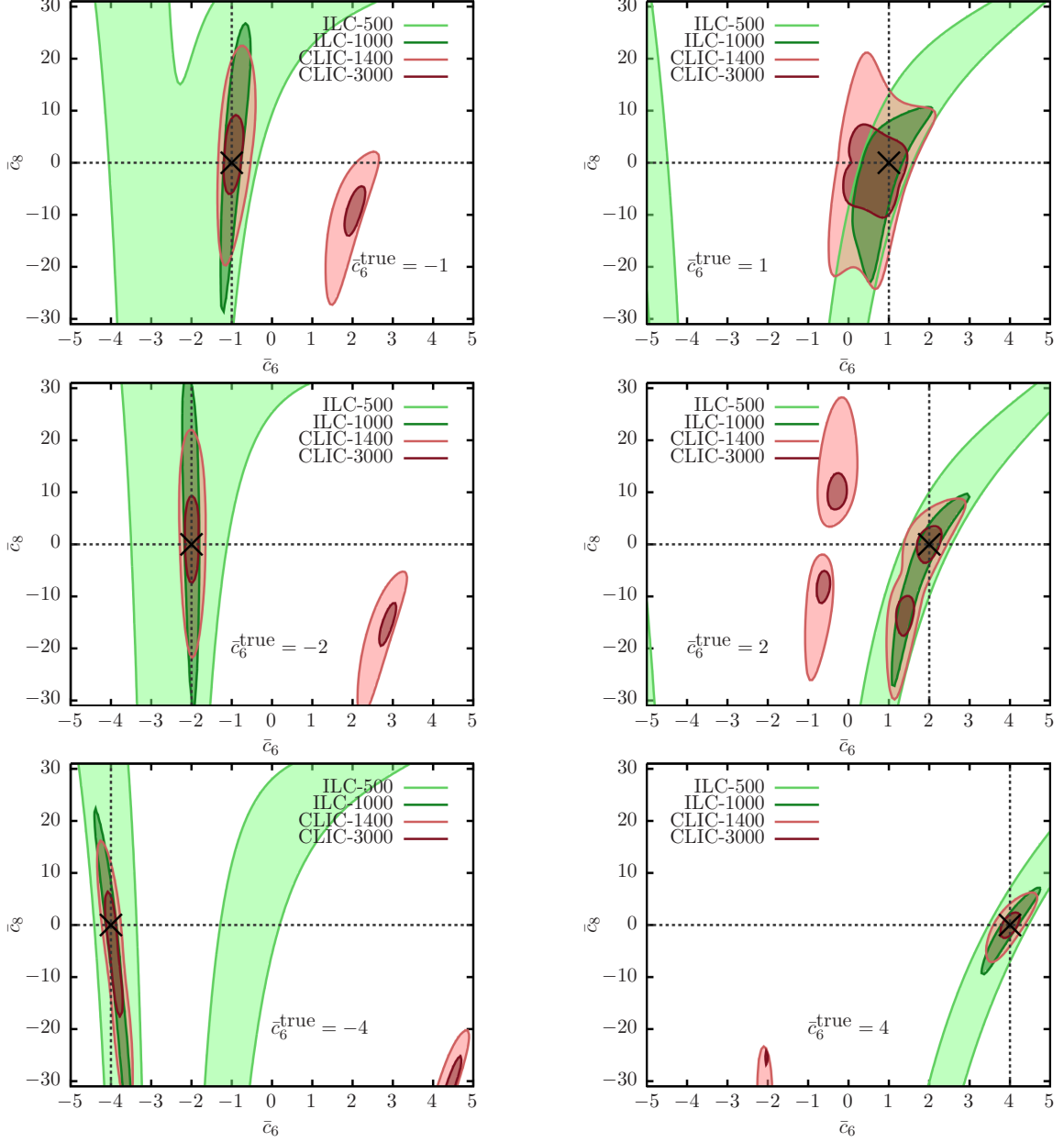


Figure 16: Combined 2σ bounds in the (\bar{c}_6, \bar{c}_8) plane assuming BSM cross sections corresponding to $(\bar{c}_6^{\text{true}}, \bar{c}_8^{\text{true}}) = (0, 0)$ in the Scenario 2 described in the text, with $\bar{c}_6^{\text{true}} = -4, -2, -1, 1, 2, 4$ marked in the plots with a cross.

future e^+e^- colliders (CEPC, FCC-ee, ILC and CLIC) and have analysed the constraints that can be set on $\bar{c}_6 \equiv \frac{c_6 v^2}{\lambda \Lambda^2}$ and $\bar{c}_8 \equiv \frac{4c_8 v^4}{\lambda \Lambda^4}$. To this purpose we have considered two scenarios:

- Scenario 1: the effects of \bar{c}_8 are negligible and we analyse the constraints that can be set on \bar{c}_6 , both for the SM potential and in the case $\bar{c}_6^{\text{true}} \neq 0$.

- Scenario 2: the effects of \bar{c}_8 are not assumed to be negligible and we analyse the constraints that can be set on the (\bar{c}_6, \bar{c}_8) plane, both for the SM potential and in the case $\bar{c}_6^{\text{true}} \neq 0$.

In Scenario 1 the value of λ_4 directly depends on λ_3 , while in Scenario 2 they are independent. We verified that requiring perturbative convergence sets upper bounds on the absolute values of \bar{c}_6 and \bar{c}_8 , *i.e.*, $|\bar{c}_6| < 5$ and $|\bar{c}_8| < 31$. Thus, we have analysed the constraints that can be set in this region of the (\bar{c}_6, \bar{c}_8) plane.

In Scenario 1, the best constraints on \bar{c}_6 can be obtained from the combination of ZH results from low-energy high-luminosity runs and results from high-energy runs for ZHH and WBF (HH, HHH) production. On the other hand, in BSM cases $\bar{c}_6^{\text{true}} \neq 0$, WBF H gives stronger constraints than ZH production and similarly WBF HH production can be more sensitive than ZHH production.

In Scenario 2, since two-loop \bar{c}_8 effects for single Higgs production are not available, we combine only double and triple Higgs production, and show the single Higgs bounds under the assumption that two-loop effects are negligible. The combination of high-energy results from double and triple Higgs production gives the best constraints and in both cases the WBF channel is in general the most relevant. Single Higgs production is only relevant for low-energy machines, and almost negligible once WBF HH is available. For this reason, the higher is the energy, the stronger are the constraints that can be obtained in the (\bar{c}_6, \bar{c}_8) plane, both for the SM case and the BSM configurations with $\bar{c}_6^{\text{true}} \neq 0$.

In both Scenario 1 and Scenario 2, although WBF HH constraints alone are stronger than those for ZHH , the two production processes are in fact complementary and lead to improved results when they are combined. At high-energy e^+e^- colliders triple Higgs production is not measurable in the SM, but its cross section strongly depends on the value of \bar{c}_8 . In particular, at CLIC-3000, the constraint that can be obtained on \bar{c}_8 via WBF HHH production are comparable to those obtainable at a future 100 TeV hadron collider.

In conclusion, we have demonstrated that the analysis of single, double and triple Higgs production at e^+e^- colliders can be exploited for constraining the trilinear and quartic coupling via direct and loop-induced indirect effects. In this first sensitivity study we have assumed that BSM effects on the couplings of the Higgs boson with other particles can be neglected. This assumption has already been shown to be reasonable for the SM case in Scenario 1 in ref. [43], yet further studies will be necessary for the other configurations considered in this work. Also, as already mentioned, another possible sensitivity on the \bar{c}_8 parameter may be obtained from the high-precision measurements of single Higgs production at future e^+e^- colliders. To establish what kind of constraints could be reached on \bar{c}_8 in this case, a two-loop computation of $e^+e^- \rightarrow ZH$ will be needed.

Acknowledgements

We acknowledge many enlightening discussions and continuous collaboration on the Higgs self-coupling determination with Giuseppe Degrandi, Christophe Grojean and Qi-Shu Yan. This work is supported in part by the “Fundamental interactions” convention FNRS-IISN

4.4517.08. This work has received funding from the European Union’s Horizon 2020 research and innovation programme as part of the Marie Skłodowska-Curie Innovative Training Network MCnetITN3 (grant agreement no. 722104) and by F.R.S.-FNRS under the “Excellence of Science - EOS” - be.h project n. 30820817. The work of D.P. is supported by the Alexander von Humboldt Foundation, in the framework of the Sofja Kovalevskaja Award Project “Event Simulation for the Large Hadron Collider at High Precision”.

A One-loop renormalisation in double Higgs production in EFT

In this section we provide all the ingredients that are necessary for one-loop renormalisation in double Higgs production with arbitrary c_6 and c_8 values. First of all, it is important to note that the only quantities that are renormalised and receive a contribution from c_6 , c_8 and c_{10} are

$$Z_H, \quad m_H, \quad T, \quad c_6, \quad (\text{A.1})$$

where Z_H is the Higgs wave function and T is the tadpole contribution, which we cancel via the δt counterterm so that the physical value of v does not get shifted. All the other quantities do not receive additional one-loop contributions on top of the SM ones, including δv , which is completely of SM origin.

Thus, for our calculation the necessary ingredients for the renormalisation of the virtual corrections are:

$$\delta Z_H = \delta Z_H^{\text{SM}} + \delta Z_H^{\text{NP}}, \quad (\text{A.2})$$

$$\delta m_H^2 = (\delta m_H^2)^{\text{SM}} + \delta(m_H^2)^{\text{NP}} - 6 \frac{c_6}{\Lambda^2} v^3 \delta v, \quad (\text{A.3})$$

$$\delta t = \delta t^{\text{SM}} + \delta t^{\text{NP}}, \quad (\text{A.4})$$

$$\delta c_6 = \delta c_6^{\text{NP}}. \quad (\text{A.5})$$

All the quantities with “SM” as apex are the SM contributions and can be found in [51], those with “NP”, which indeed stands for new physics, are the new contributions from c_6 , c_8 and c_{10} . Besides c_6 , which is renormalised in the $\overline{\text{MS}}$ scheme, all the other EW input parameters are assumed to be renormalised on-shell, with exception of fine structure α , which we renormalise in the G_μ -scheme. This is relevant for our calculation since in the SM the renormalisation of v is related to the charge renormalisation, δZ_e ,

$$\frac{\delta v}{v} = \frac{\delta s_W}{s_W} - \delta Z_e + \frac{\delta m_W^2}{2m_W^2}. \quad (\text{A.6})$$

The appearance of the extra quantity $-6 \frac{c_6}{\Lambda^2} v^3 \delta v$ in eq. (A.3) is due to the presence of v in the parametrisation of eq. (2.2), which as we said has an impact in the renormalisation procedure. Before giving the explicit formulas for δZ_H^{NP} , $\delta(m_H^2)^{\text{NP}}$, δt^{NP} and the counterterm for the H^3 vertex and H propagator, we briefly discuss this technical aspect.

The explicit term v used in the parametrisation of eq. (2.2) is a subtle quantity. In a tree-level analysis it can be trivially identified with the location of the minimum of $V(\Phi)$, which defines the ground state $|0\rangle$ of the Higgs field

$$|\langle 0 | \Phi | 0 \rangle|^2 = \frac{v^2}{2}. \quad (\text{A.7})$$



$$\text{---}\times\text{---} = \delta\lambda_{H^3} \quad (\text{A.8})$$

Figure 17: The counter term for the triple Higgs vertex.

However, strictly speaking, the v appearing in eq. (2.2) is, like Λ , just a mass parameter that we chose for mapping c'_{2n} into c_{2n} . In principle we could have chosen a generic mass $M \neq v$, but we would have not got any advantage. On the contrary, with $M = v$, SM relations such as

$$\delta\lambda = \frac{\delta m_H^2}{2v^2} - \frac{m_H^2 \delta v}{v^3} + \frac{\delta t}{2v^3}, \quad (\text{A.9})$$

$$\delta v = \delta v^{\text{SM}} \leftrightarrow \delta v^{\text{NP}} = 0, \quad (\text{A.10})$$

are preserved (see ref. [61]); they would be different using eq. (2.3). The crucial point is that at one loop, or even at higher orders, $|\langle 0|\Phi|0\rangle|$ is involved in the renormalisation, while the term v in eq. (2.2) is not; as said it is just a mass parameter tuned to v for our purpose. For this reason, relations among the different renormalisation constant of the SM parameters are unaltered, but in the case of m_H and H^n vertexes the definitions of the renormalisation counterterms contain additional terms.

This mechanism is at the origin of the aforementioned term in eq. (A.3) as well as to some additional terms (second line of eq. (A.11)) that appear in the counterterm for the H^3 vertex in Fig. 17, where $\delta\lambda_{H^3}$ reads

$$\begin{aligned} \delta\lambda_{H^3} = & -i6 \left[\frac{c_6 v^3}{\Lambda^2} \left(\frac{\delta c_6}{c_6} + \frac{3}{2} \delta Z_H + 3 \frac{\delta v}{v} \right) + \lambda v \left(\frac{\delta \lambda}{\lambda} + \frac{3}{2} \delta Z_H + \frac{\delta v}{v} \right) \right] \\ & -i6 \left[\frac{4c_8 v^4 \delta v}{\Lambda^4} + 3 \frac{c_6}{\Lambda^2} v^2 \delta v \right]. \end{aligned} \quad (\text{A.11})$$

Similarly, the Feynman rule for the counterterm of the Higgs propagator (see eq. (A.4) in ref. [51]) is modified into

$$\text{---}\times\text{---} = -i \left(\delta m_H^2 + m_H^2 \delta Z_H - \delta Z_H k^2 + 6 \frac{c_6}{\Lambda^2} v^3 \delta v \right), \quad (\text{A.12})$$

and therefore the additional term entering in eq. (A.3) is exactly canceled.

The only missing information are the NP contributions to the counterterms in eqs. (A.2)-(A.4), which we thus provide in the following:

$$\delta t^{\text{NP}} = -\frac{1}{16\pi^2} \frac{3c_6}{\Lambda^2} v^3 A_0(m_H^2), \quad (\text{A.13})$$

$$\delta Z_H^{\text{NP}} = \left(\frac{2c_6 v^2}{\lambda \Lambda^2} + \frac{c_6^2 v^4}{\lambda^2 \Lambda^4} \right) \delta Z_H^{\text{SM}, \lambda}, \quad (\text{A.14})$$

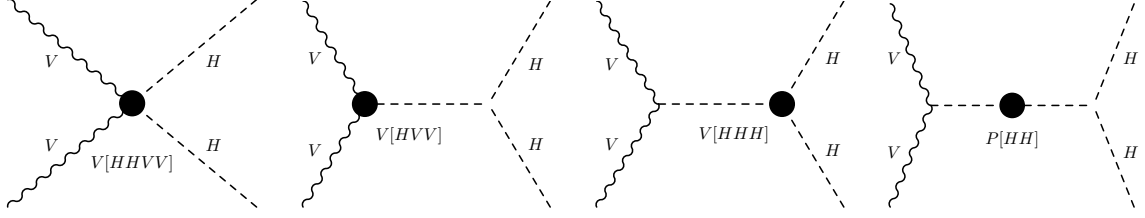


Figure 18: The structure of one-loop effects in the $HHVV$ amplitude expressed via form factors.

$$\delta(m_H^2)^{\text{NP}} = \frac{1}{16\pi^2} \left[\frac{c_6}{\Lambda^2} v^2 (18A_0(m_H^2) + 3A_0(\xi_Z m_Z^2) + 6A_0(\xi_W m_W^2) + 18m_H^2 B_0(m_H^2, m_H^2, m_H^2)) + \right. \\ \left. + \frac{v^4}{\Lambda^4} (12c_8 A_0(m_H^2) + c_6^2 18v^2 B_0(m_H^2, m_H^2, m_H^2)) \right], \quad (\text{A.15})$$

$$\delta c_6 = \frac{\Delta}{16\pi^2} \left[c_6 \left(54\lambda - 9 \frac{m_Z^2 + 2m_W^2}{v^2} + 6 \frac{N_c m_t^2}{v^2} \right) + \frac{c_8 v^2}{\Lambda^2} \left(64\lambda - 6 \frac{m_Z^2 + 2m_W^2}{v^2} + 4 \frac{N_c m_t^2}{v^2} \right) + \frac{45c_6^2 v^2}{\Lambda^2} + \frac{20c_{10}\lambda v^4}{\Lambda^4} + \frac{36c_6 c_8 v^4}{\Lambda^4} \right], \quad (\text{A.16})$$

where

$$\delta Z_H^{\text{SM},\lambda} = -\frac{9\lambda m_H^2}{16\pi^2} B'_0(m_H^2, m_H^2, m_H^2) \quad (\text{A.17})$$

is the contribution from the trilinear Higgs self-coupling to δZ_H in the SM and A_0 and B_0 are the standard scalar loop integrals and Δ is the UV divergence $\Delta \equiv 1/\epsilon - \gamma + \log(4\pi)$ in $D = 4 - 2\epsilon$ dimensions. As discussed in sec. 3.2 terms up to the order $(v/\Lambda)^6$ have to be in general considered. However, note that no terms beyond $(v/\Lambda)^2$ are present in δt , or beyond $(v/\Lambda)^4$ in δZ_H and δm_H^2 , while c_6 is appearing at order $(v/\Lambda)^2$, so terms up to $(v/\Lambda)^6$ are in fact present in δc_6 .

We want to stress that all these contributions have to be taken into account in order to obtain gauge invariance for the final finite result of double-Higgs production at one loop. We kept the explicit dependence on the ξ parameter for a generic R_ξ -gauge in order to verify that renormalised amplitudes do not depend on ξ . With this calculation setup, results are equivalent to those of a standard calculations based on the parameterisation of eq. (2.3) and c'_{2n} coefficients renormalised in the $\overline{\text{MS}}$ scheme.

B One-loop amplitudes via form factors

In this section we provide all the form factors that are necessary for the calculations of one-loop amplitudes for ZHH and WBF HH production entering $\sigma_{\text{NLO}}^{\text{pheno}}(HH)$ in eq. (3.21). These are the form factors for the

- HVV vertex,
- HHH vertex,

- $HHVV$ vertex,
- H propagator.

We include contributions up to the order $(v/\Lambda)^6$ and therefore one-loop amplitudes entering $\sigma_{\text{NLO}}^{\text{pheno}}(HH)$ can be obtained by substituting the vertexes in the corresponding tree-level amplitudes with the aforementioned form factors. Indeed, we implemented them in a UFO [62] model file and performed the calculation within the MADGRAPH5_AMC@NLO [63] framework²¹, as also done in ref. [40]. We cross-checked the results via FEYNARTS 3.9 [64] and FORMCALC 9.4 [65]. Loops integrals have been evaluated with LOOPTOOLS 2.13 [65] and QCDLOOP 2.0.3 [66, 67].

The HVV form factor is the only one that is also relevant for the calculation of one-loop amplitudes entering $\sigma_{\text{NLO}}^{\text{pheno}}(H)$ for single Higgs production. For this kind of processes the $(\bar{c}_6)^2$ dependence originates completely from δZ_H^{NP} in eq. (A.14), while the linear term in \bar{c}_6 comes from both δZ_H^{NP} and the HVV form factor, which has already been calculated in ref. [37] and induces the C_1 dependence on the kinematics. We repeated the calculation explicitly checking the gauge invariance, both for a generic R_ξ gauge and also in unitary gauge.

Before providing the expressions for the different form factors we want to briefly show how the calculation of the σ_{30} , σ_{40} , σ_{01} , σ_{11} and σ_{21} terms, which are part of $\sigma_{\text{NLO}}^{\text{pheno}}(HH)$, can be organised. As said, the form factors provided in the following can be plugged into the tree-level diagrams in order to get the necessary one-loop amplitudes for ZHH and WBF HH giving $\sigma_{\text{NLO}}^{\text{pheno}}(HH)$. This is schematically depicted in Fig. 18, where the relevant part of the ZHH and WBF HH amplitudes, respectively $W^*W^* \rightarrow HH$ or $Z^* \rightarrow HHZ$, is shown. Via the interference of tree-level amplitudes and such one-loop amplitudes obtained via form factors, we would get a cross section that we denote as σ^{FF} , where FF stands for form-factors. It is important to note that σ^{FF} contains also \bar{c}_6 - and $(\bar{c}_6)^2$ -dependent spurious terms, which have to be discarded. One can easily expand in powers of $\bar{c}_6^i \bar{c}_8^j$ the σ^{FF} result and identify the different σ_{ij}^{FF} component.

We should note that for consistency we provide the form factor of HVV matching the same convention used in ref. [37], *i.e.*, without including the contribution of the Higgs wave-function counterterm δZ_H^{NP} . The same convention is used also for all the other form-factors. Note that in the case of the H propagator and HHH vertex, UV divergences are present in the terms relevant for our calculation and thus the other UV counterterms have to be included in the definition of the form-factors. In conclusion the actual σ_{ij} components can be expressed in terms of the σ_{ij}^{FF} as

$$\sigma_{01,11,21} = \sigma_{01,11,21}^{\text{FF}}, \quad (\text{B.1})$$

$$\sigma_{30} = \sigma_{30}^{\text{FF}} + 2\delta Z_H^{\text{SM},\lambda} \sigma_1 + 4\delta Z_H^{\text{SM},\lambda} \sigma_2, \quad (\text{B.2})$$

$$\sigma_{40} = \sigma_{40}^{\text{FF}} + 2\delta Z_H^{\text{SM},\lambda} \sigma_2, \quad (\text{B.3})$$

²¹We have used the version 2.4.3 of this code, but we could have in principle used also a more or less recent version of it.

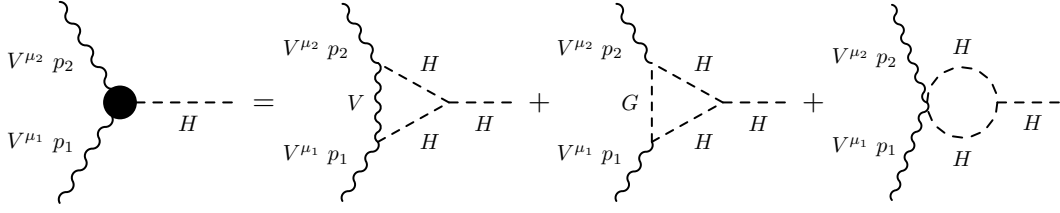


Figure 19: Feynman diagrams contributing to the $V[HV V]$ form factor at one loop.

where σ_1 and σ_2 are part of $\sigma_{\text{LO}}(HH)$ in eq. (3.10). Note that σ_{30} and σ_{40} are written in such a form that can be easily extend to the case in which the δZ_H^{NP} contribution from external legs is resummed, as done in ref. [36]. However, considering $|\bar{c}_6| < 5$, resummation is not necessary given that $\bar{c}_6^2 \delta Z_H^{\text{SM},\lambda} < 4\%$.

HV V-vertex

The HVV form factor, which will denote as $V[HV V]$, enters both the single and double Higgs production calculation and can be written as

$$V^{\mu_1\mu_2}[HV V] = V_0^{\mu_1\mu_2}[HV V] + V_1^{\mu_1\mu_2}[HV V]\bar{c}_6. \quad (\text{B.4})$$

For our calculation the \bar{c}_6 -independent part can be ignored, while in a generic gauge $V_1[HV V]$ is given by the three diagrams ²² in Fig. 19. Using the convention that the corresponding Feynman rule is $iV^{\mu_1\mu_2}[HV V]$, as we will do also for the other form factors, we can write $V_1^{\mu_1\mu_2}[HV V]$ as

$$V_1^{\mu_1\mu_2}[HV V] = \frac{\lambda m_V^2}{16\pi^2 v} T^{\mu_1\mu_2}(p_1, p_2, m_V, m_H). \quad (\text{B.5})$$

In particular

$$T^{\mu_1\mu_2}(p_1, p_2, m_V, m_H) = (-6B_0 - 24m_V^2 C_0 + 24C_{00})g^{\mu_1\mu_2} - 24p_1^{\mu_2} p_2^{\mu_1} C_{12}, \quad (\text{B.6})$$

where p_1, p_2 are the (incoming) momenta of the two vector bosons, μ_1, μ_2 are the corresponding Lorentz indices, m_V with $V = W, Z$ is mass of the vector bosons, and B_0, C_0, C_{00}, C_{12} are one-loop scalar/tensor integrals defined according to the notation used, *e.g.*, in ref. [51] and where the following variables are understood:

$$B_0 = B_0((p_1 + p_2)^2, m_H^2, m_H^2), \quad (\text{B.7})$$

$$C_{0,00,12} = C_{0,00,12}(p_1^2, (p_1 + p_2)^2, p_2^2, m_V^2, m_H^2, m_H^2). \quad (\text{B.8})$$

We remind the reader that the $\frac{1}{2}\delta Z_H^{\text{NP}}$ contribution from the external H has been removed from $V[HV V]$.

²²In the unitary gauge the second diagram does not appear

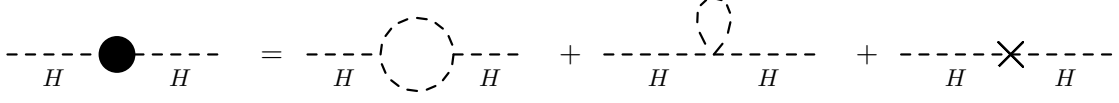


Figure 20: Feynman diagrams contributing to $P[HH]$.

H propagator

The form factors for the HH two point function, which we denote as $P[HH]$, receives one-loop contributions from the diagrams in Fig. 20, where the contribution of counterterm diagram is given in eq. (A.12). At one loop $P[HH]$ can be written as

$$P[HH] = P_{00}[HH] + P_{10}[HH]\bar{c}_6 + P_{20}[HH]\bar{c}_6^2. \quad (\text{B.9})$$

In our calculation we do not include $P_{00}[HH]$ contributions, which we set to zero, while $P_{10}[HH]$ and $P_{20}[HH]$ read

$$P_{10}[HH] = 2P_{20}[HH] = \frac{1}{16\pi^2}(6\lambda v)^2 [B_0(p^2, m_H^2, m_H^2) - B_0(m_H^2, m_H^2, m_H^2)], \quad (\text{B.10})$$

It is important to note that $P(HH)$ does not depend on \bar{c}_8 . Indeed, although the second diagram, the seagull, depends on \bar{c}_8 due to the $HHHH$ vertex, it is exactly cancelled by the Higgs-mass counter term. We remind the reader that the $-\delta Z_H^{\text{NP}}$ component in the counterterm has been removed from $P[HH]$.

HHH-vertex form factor

The form-factor for the HHH vertex, $V[HHH]$, receives contributions from the diagrams already shown in the main text in Fig. 4 and the counter term of Fig. 17. At variance with $V[HV V]$ and $P[HH]$, $V[HHH]$ depends on both \bar{c}_6 and \bar{c}_8 :

$$V[HHH] = \sum_{i+2j \leq 3} V_{ij}[HHH] \bar{c}_6^i \bar{c}_8^j. \quad (\text{B.11})$$

For our calculation $V_{00}[HHH]$ and $V_{10}[HHH]$ can be set equal to zero, while

$$V_{30}[HHH] = \frac{1}{16\pi^2} (6\lambda v)^3 C_0(p_1^2, p_2^2, p_3^2, m_H^2, m_H^2, m_H^2), \quad (\text{B.12})$$

$$V_{20}[HHH] = \frac{1}{16\pi^2} (6\lambda v)^3 3C_0(p_1^2, p_2^2, p_3^2, m_H^2, m_H^2, m_H^2), \quad (\text{B.13})$$

$$+ \frac{1}{16\pi^2} 108\lambda^2 v \left\{ -\frac{1}{2} [B_0(m_H^2, m_H^2, m_H^2) - \Delta] + \sum_{i=1}^3 [B_0(p_i^2, m_H^2, m_H^2) - \Delta] \right\},$$

$$V_{01}[HHH] = \frac{\lambda v}{16\pi^2} \left\{ 18\lambda \left[\sum_{i=1}^3 [B_0(p_i^2, m_H^2, m_H^2) - \Delta] \right] - 6 \left[\frac{N_c m_t^2}{v^2} \Delta + 16\pi^2 \frac{\delta v}{v} \right] \right. \quad (\text{B.14})$$

$$\left. + 21 \frac{A_0(m_H^2) - m_H^2 \Delta}{v^2} + 3 \frac{A_0(\xi_Z m_Z^2) + 3m_Z^2 \Delta}{v^2} + 6 \frac{A_0(\xi_W m_W^2) + 3m_W^2 \Delta}{v^2} \right\},$$

$$V_{11}[HHH] = \frac{\lambda v}{16\pi^2} 18\lambda \left[\sum_{i=1}^3 [B_0(p_i^2, m_H^2, m_H^2) - \Delta] \right], \quad (\text{B.15})$$

where the B_0 and C_0 are the loop scalar integrals, with the dependence on external momenta and internal masses expressed with the convention in ref. [51]. The term Δ is the UV divergence as defined in Appendix A. The $V_{30}[HHH]$ component is equivalent to the result of ref. [56], where it is assumed $V[HHH] \sim (1 + \bar{c}_6)^3 V_{30}[HHH]$. It should be noticed that the contribution of δv , which as discussed in Appendix A is completely of SM origin, is necessary in order to obtain UV finiteness and gauge-invariance for the finite results. We kept the explicit dependence on the ξ gauge parameters outside δv precisely to make this point manifest. In order to help the reader we report in the following the UV divergent part of δv and the ξ -dependent part, which includes both finite and divergent contributions

$$(\delta v)^{\text{UV}} = (\delta v^{\text{SM}})^{\text{UV}} = \frac{\Delta}{16\pi^2} \left[\frac{1}{2} \frac{(3 + \xi_Z)m_Z^2 + 2(3 + \xi_W)m_W^2}{v} - \frac{N_c m_t^2}{v} \right], \quad (\text{B.16})$$

$$(\delta v)_\xi = (\delta v^{\text{SM}})_\xi = \frac{1}{16\pi^2} \frac{1}{2v} [A_0(m_Z^2 \xi_Z) + 2A_0(m_W^2 \xi_W)]. \quad (\text{B.17})$$

We remind the reader that the $\frac{3}{2}\delta Z_H^{\text{NP}}$ component in the counterterm, which originates from the three H external legs, has been removed from $V[HHH]$.

HHVV-vertex form factor

Similarly to the case of $V[HHH]$, the form factor for the $HHVV$ vertex, $V[HHVV]$, can be written as

$$V[HHVV] = \sum_{i+2j \leq 2} V_{ij}[HHVV] \bar{c}_6^i \bar{c}_8^j. \quad (\text{B.18})$$

For our calculation only $V_{20}[HHVV]$ and $V_{01}[HHVV]$ are relevant and we set the other contributions to zero. The $V_{01}[HHVV]$ component originates from the diagrams in Fig. 21 and its structure is very similar to the one of $V_1[HV V]$,

$$V_{01}^{\mu_1 \mu_2}[HHVV] = \frac{\lambda m_V^2}{16\pi^2 v^2} T^{\mu_1 \mu_2}(p_1, p_2, m_V, m_H), \quad (\text{B.19})$$

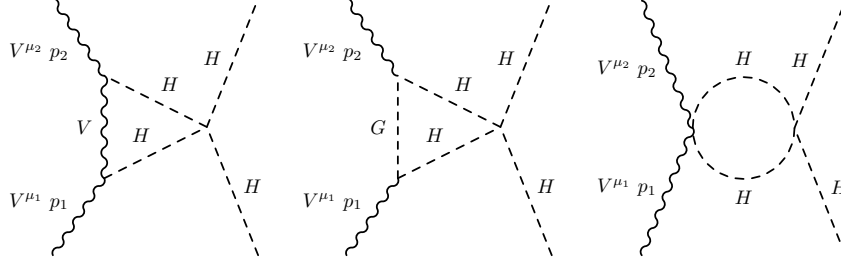


Figure 21: Feynman diagrams contributing to the $V_{01}[HHVV]$ form factor.

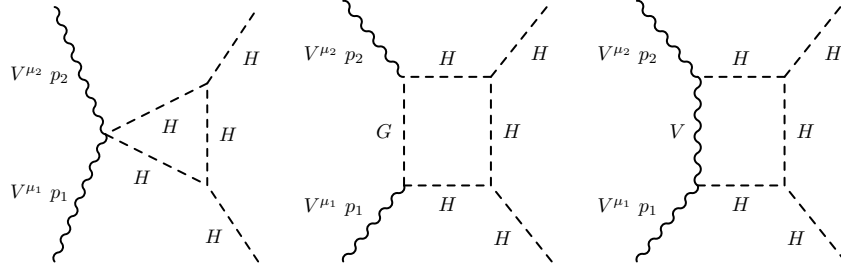


Figure 22: Representative Feynman diagrams contributing to the $V_{20}[HHVV]$ form factor.

where all momentum are incoming and $T^{\mu_1\mu_2}$ is given in eq. (B.6). The $V_{20}[HHVV]$ term instead originates from the diagrams in Fig. 22, which include boxes and thus they involve a much more complex kinematic dependence,

$$V_{20}^{\mu_1\mu_2}[HHVV] = 9 \frac{\lambda^2 m_V^2}{\pi^2} [F^{\mu_1\mu_2}(p_1, p_2, p_3, p_4, m_V, m_H) + F^{\mu_1\mu_2}(p_1, p_2, p_4, p_3, m_V, m_H)], \quad (\text{B.20})$$

where $F^{\mu_1\mu_2}$ is given by

$$\begin{aligned} F^{\mu_1\mu_2}(p_1, p_2, p_3, p_4, m_V, m_H) = & \left(-\frac{1}{4}C_0 - m_V^2 D_0 + D_{00}\right) g^{\mu_1\mu_2} + p_4^{\mu_1} p_1^{\mu_2} D_{12} \\ & + p_4^{\mu_1} (p_1 + p_4)^{\mu_2} D_{22} - p_2^{\mu_1} p_1^{\mu_2} D_{13} - p_2^{\mu_1} (p_1 + p_4)^{\mu_2} D_{23}, \end{aligned} \quad (\text{B.21})$$

with the dependence on external momenta and internal masses of C and D functions as

$$C_0 = C_0((p_3 + p_4)^2, p_3^2, p_4^2, m_H^2, m_H^2, m_H^2), \quad (\text{B.22})$$

$$D_{i(j)} = D_{i(j)}(p_1^2, p_4^2, p_3^2, p_2^2, (p_1 + p_4)^2, (p_4 + p_3)^2, m_V^2, m_H^2, m_H^2, m_H^2), \quad (\text{B.23})$$

according to the convention of ref. [51]. Both $V_{01}[HHVV]$ and $V_{20}[HHVV]$ are UV finite and gauge-invariant. We remind the reader that the δZ_H^{NP} component in the counterterm, which originates from the two H external legs, has been removed from $V[HHVV]$.

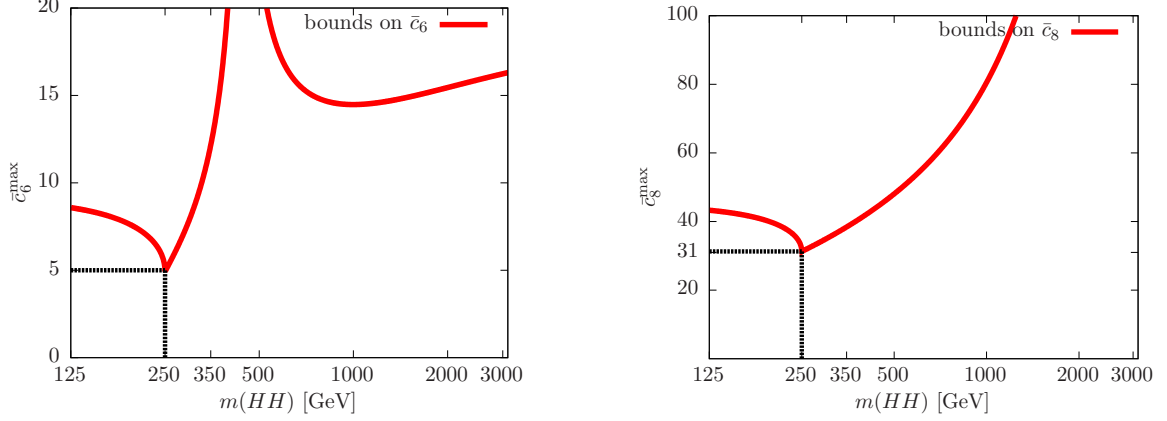


Figure 23: Maximum value of \bar{c}_6 (left) and \bar{c}_8 (right) such that the one-loop corrections to the HHH amplitude are smaller than its tree-level value. We consider two Higgs bosons on-shell and the third with virtuality equal to $m(HH)$, showing the dependence on $m(HH)$.

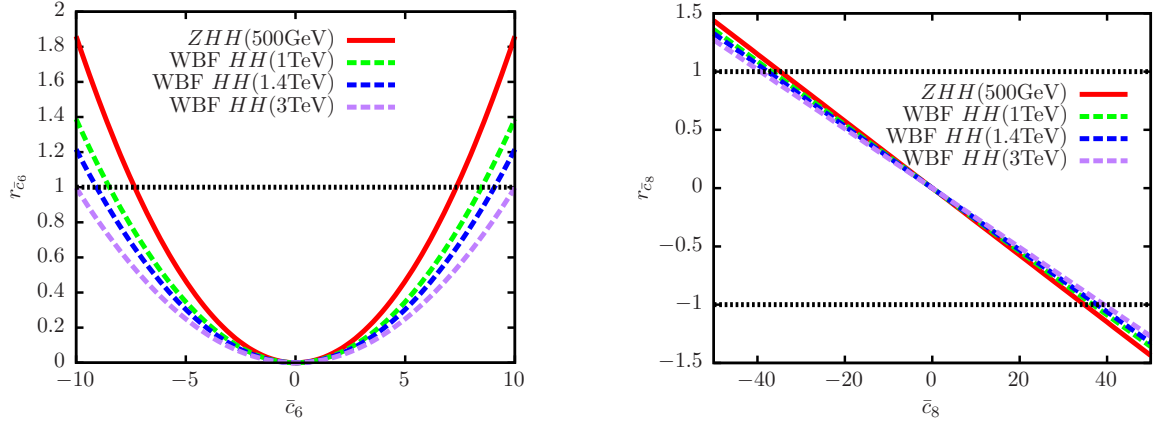


Figure 24: \bar{c}_6 -dependence of $r_{\bar{c}_6}$ (left) and \bar{c}_8 -dependence of $r_{\bar{c}_8}$ (right) for ZHH and $WBF HH$ at different energies.

C Perturbative limits on \bar{c}_6 and \bar{c}_8 in double Higgs production

In this section we describe how we derived the range of validity of our calculation,

$$|\bar{c}_6| < 5 \quad \text{and} \quad |\bar{c}_8| < 31, \quad (\text{C.1})$$

which has already mentioned several times in the text.

First of all, we analyse the one-loop $H^* \rightarrow HH$ amplitude, the analytical expression of which can be obtained via δZ_H^{NP} and the form factors $P[HH]$ and the $V[HHH]$ that have been provided in the previous section. We define as $\bar{c}_6^{\text{max}}(\bar{c}_8^{\text{max}})$ the value of $\bar{c}_6(\bar{c}_8)$ such that the one-loop amplitude is as large as the tree-level one, *i.e.* the value of $\bar{c}_6(\bar{c}_8)$ from where perturbative convergence cannot be trusted anymore. For the estimation of \bar{c}_6^{max} we take into account the leading contribution from V_{30} and P_{20} , both yielding \bar{c}_6^3 terms. For

\bar{c}_8^{\max} we instead consider as first step the contribution from V_{11} , which is the dominant term when \bar{c}_6 is large, and we compare it with the linearly \bar{c}_6 dependent part of the tree-level vertex. In such a way the value of \bar{c}_8^{\max} is independent on \bar{c}_6 .

The value of $\bar{c}_6^{\max}(\bar{c}_8^{\max})$ has a kinematic dependence. In the left plot of Fig. 23 we display the dependence of \bar{c}_6^{\max} on $m(HH)$, ranging from 125 GeV to 3 TeV. The equivalent plot for \bar{c}_8^{\max} , taking leading term in \bar{c}_6 , is shown on the right. Thus, we explore $m(HH)$ values both below the production threshold and in the tail of the $m(HH)$ distributions. As can be seen in both cases, the most stringent constraints, $|\bar{c}_6| < 5$ and $|\bar{c}_8| < 31$, arise from the threshold condition $m(HH) = 2m_H$, while for different values of $m(HH)$ the bound is weaker.

In the case of \bar{c}_6^{\max} the constraint is independent on the value of the renormalisation scale μ_r and compatible with the result obtained in ref. [56], where the subdominant contribution of P_{20} was not taken into account. Conversely, in the case of \bar{c}_8^{\max} the constraint does depend on the value of the renormalisation scale μ_r . However, we verified for $\mu_r = m_H, 4m_H$, that the most stringent \bar{c}_8^{\max} value is anyway arising from the kinematic condition $m(HH) = 2m_H$.

The constraints of eq. (C.1) have been derived via the analysis of the $H^* \rightarrow HH$ amplitude, but also the HVV and $HHVV$ vertexes contribute via loop corrections to the quantity $\sigma_{\text{NLO}}^{\text{pheno}}(HH)$, eq. (3.21), that is used for our phenomenological analysis. Thus, it is important to check if they can affect the results of eq. (C.1). To this purpose we directly considered the quantities

$$\begin{aligned} r_{\bar{c}_6} &\equiv \frac{\bar{c}_6^4 \sigma_{40}}{\bar{c}_6^2 \sigma_2} = \frac{\sigma_{40}}{\sigma_2} \bar{c}_6^2, \\ r_{\bar{c}_8} &\equiv \frac{\sigma_{21} \bar{c}_6^2 \bar{c}_8}{\sigma_2 \bar{c}_6^2} = \frac{\sigma_{21}}{\sigma_2} \bar{c}_8, \end{aligned} \quad (\text{C.2})$$

for $ZHHH$ and WBF HH at different energies. The quantity $r_{\bar{c}_6}$ is the ratio between the term with the highest power in \bar{c}_6 from $\Delta\sigma_{\bar{c}_6}$ and the one with the highest power in \bar{c}_6 from σ_{LO} , *i.e.*, the ratio of the dominant contributions at tree and one-loop level for large \bar{c}_6 values. Similarly, the quantity $r_{\bar{c}_8}$ is the ratio between the term with the highest power in \bar{c}_6 from $\Delta\sigma_{\bar{c}_8}$ and σ_{LO} . Thus, both of them can be considered as a generalisation of the first step; both HVV and $HHVV$ vertices are taken into account and phase-space integration is performed.

In the left plot of Fig. 24, we show $r_{\bar{c}_6}$ for the case of ZHH at 500 GeV and of WBF at 1, 1.4 and 3 TeV, which are the phenomenologically relevant scenarios analysed in sec. 4. Requiring $|r_{\bar{c}_6}| < 1$, we can get $|\bar{c}_6| < 8$ for ZHH at 500 GeV, and $|\bar{c}_6| < 9, 10, 11$ for WBF HH at 1000, 1400 and 3000 GeV, respectively. Thus, as one would expected from Fig. 23 for the $H^* \rightarrow HH$ vertex, at higher energies, far from the production threshold, limits are weaker. In the right plot we show $r_{\bar{c}_8}$ for the same energies and process. Also in this case the obtained limits are weaker than in eq. (C.1), $|\bar{c}_8| < \sim 35 - 40$.

References

- [1] **CMS** Collaboration, S. Chatrchyan *et al.*, *Observation of a new boson at a mass of 125 GeV with the CMS experiment at the LHC*, *Phys. Lett.* **B716** (2012) 30–61, [[1207.7235](#)].
- [2] **ATLAS** Collaboration, G. Aad *et al.*, *Observation of a new particle in the search for the Standard Model Higgs boson with the ATLAS detector at the LHC*, *Phys. Lett.* **B716** (2012) 1–29, [[1207.7214](#)].
- [3] **ATLAS, CMS** Collaboration, G. Aad *et al.*, *Measurements of the Higgs boson production and decay rates and constraints on its couplings from a combined ATLAS and CMS analysis of the LHC pp collision data at $\sqrt{s} = 7$ and 8 TeV*, *JHEP* **08** (2016) 045, [[1606.02266](#)].
- [4] U. Baur, T. Plehn, and D. L. Rainwater, *Probing the Higgs selfcoupling at hadron colliders using rare decays*, *Phys. Rev.* **D69** (2004) 053004, [[hep-ph/0310056](#)].
- [5] M. J. Dolan, C. Englert, and M. Spannowsky, *Higgs self-coupling measurements at the LHC*, *JHEP* **10** (2012) 112, [[1206.5001](#)].
- [6] A. Papaefstathiou, L. L. Yang, and J. Zurita, *Higgs boson pair production at the LHC in the $b\bar{b}W^+W^-$ channel*, *Phys. Rev.* **D87** (2013), no. 1 011301, [[1209.1489](#)].
- [7] J. Baglio, A. Djouadi, R. Gröber, M. M. Mühlleitner, J. Quevillon, and M. Spira, *The measurement of the Higgs self-coupling at the LHC: theoretical status*, *JHEP* **04** (2013) 151, [[1212.5581](#)].
- [8] W. Yao, *Studies of measuring Higgs self-coupling with $HH \rightarrow b\bar{b}\gamma\gamma$ at the future hadron colliders*, in *Proceedings, 2013 Community Summer Study on the Future of U.S. Particle Physics: Snowmass on the Mississippi (CSS2013): Minneapolis, MN, USA, July 29-August 6, 2013*, 2013. [1308.6302](#).
- [9] V. Barger, L. L. Everett, C. B. Jackson, and G. Shaughnessy, *Higgs-Pair Production and Measurement of the Triscalar Coupling at LHC(8,14)*, *Phys. Lett.* **B728** (2014) 433–436, [[1311.2931](#)].
- [10] D. E. Ferreira de Lima, A. Papaefstathiou, and M. Spannowsky, *Standard model Higgs boson pair production in the $(b\bar{b})(b\bar{b})$ final state*, *JHEP* **08** (2014) 030, [[1404.7139](#)].
- [11] C. Englert, F. Krauss, M. Spannowsky, and J. Thompson, *Di-Higgs phenomenology in $t\bar{t}hh$: The forgotten channel*, *Phys. Lett.* **B743** (2015) 93–97, [[1409.8074](#)].
- [12] D. Wardrope, E. Jansen, N. Konstantinidis, B. Cooper, R. Falla, and N. Norjoharuddeen, *Non-resonant Higgs-pair production in the $b\bar{b}b\bar{b}$ final state at the LHC*, *Eur. Phys. J.* **C75** (2015), no. 5 219, [[1410.2794](#)].
- [13] T. Liu and H. Zhang, *Measuring Di-Higgs Physics via the $t\bar{t}hh \rightarrow t\bar{t}b\bar{b}b\bar{b}$ Channel*, [1410.1855](#).
- [14] A. Azatov, R. Contino, G. Panico, and M. Son, *Effective field theory analysis of double Higgs boson production via gluon fusion*, *Phys. Rev.* **D92** (2015), no. 3 035001, [[1502.00539](#)].
- [15] Q. Li, Z. Li, Q.-S. Yan, and X. Zhao, *Probe Higgs boson pair production via the $3\ell 2j + \text{missing } E_T$ mode*, *Phys. Rev.* **D92** (2015), no. 1 014015, [[1503.07611](#)].
- [16] C.-T. Lu, J. Chang, K. Cheung, and J. S. Lee, *An exploratory study of Higgs-boson pair production*, *JHEP* **08** (2015) 133, [[1505.00957](#)].
- [17] Q.-H. Cao, B. Yan, D.-M. Zhang, and H. Zhang, *Resolving the Degeneracy in Single Higgs Production with Higgs Pair Production*, *Phys. Lett.* **B752** (2016) 285–290, [[1508.06512](#)].

- [18] Q.-H. Cao, Y. Liu, and B. Yan, *Measuring trilinear Higgs coupling in WHH and ZHH productions at the high-luminosity LHC*, *Phys. Rev.* **D95** (2017), no. 7 073006, [[1511.03311](#)].
- [19] J. K. Behr, D. Bortoletto, J. A. Frost, N. P. Hartland, C. Issever, and J. Rojo, *Boosting Higgs pair production in the $b\bar{b}b\bar{b}$ final state with multivariate techniques*, *Eur. Phys. J.* **C76** (2016), no. 7 386, [[1512.08928](#)].
- [20] Q.-H. Cao, G. Li, B. Yan, D.-M. Zhang, and H. Zhang, *Double Higgs production at the 14 TeV LHC and a 100 TeV pp collider*, *Phys. Rev.* **D96** (2017), no. 9 095031, [[1611.09336](#)].
- [21] A. Adhikary, S. Banerjee, R. K. Barman, B. Bhattacharjee, and S. Niyogi, *Revisiting the non-resonant Higgs pair production at the HL-LHC*, [[1712.05346](#)].
- [22] CMS Collaboration, C. Collaboration, *Search for Higgs boson pair production in the final state containing two photons and two bottom quarks in proton-proton collisions at $\sqrt{s} = 13$ TeV*.
- [23] *Prospects for measuring Higgs pair production in the channel $H(\rightarrow \gamma\gamma)H(\rightarrow b\bar{b})$ using the ATLAS detector at the HL-LHC*, Tech. Rep. ATL-PHYS-PUB-2014-019, CERN, Geneva, Oct, 2014.
- [24] T. Plehn and M. Rauch, *The quartic higgs coupling at hadron colliders*, *Phys. Rev.* **D72** (2005) 053008, [[hep-ph/0507321](#)].
- [25] T. Binoth, S. Karg, N. Kauer, and R. Ruckl, *Multi-Higgs boson production in the Standard Model and beyond*, *Phys. Rev.* **D74** (2006) 113008, [[hep-ph/0608057](#)].
- [26] F. Maltoni, E. Vryonidou, and M. Zaro, *Top-quark mass effects in double and triple Higgs production in gluon-gluon fusion at NLO*, *JHEP* **11** (2014) 079, [[1408.6542](#)].
- [27] J. Baglio, A. Djouadi, and J. Quevillon, *Prospects for Higgs physics at energies up to 100 TeV*, *Rept. Prog. Phys.* **79** (2016), no. 11 116201, [[1511.07853](#)].
- [28] C.-Y. Chen, Q.-S. Yan, X. Zhao, Y.-M. Zhong, and Z. Zhao, *Probing triple-Higgs productions via $4b2\gamma$ decay channel at a 100 TeV hadron collider*, *Phys. Rev.* **D93** (2016), no. 1 013007, [[1510.04013](#)].
- [29] W. Kilian, S. Sun, Q.-S. Yan, X. Zhao, and Z. Zhao, *New Physics in multi-Higgs boson final states*, *JHEP* **06** (2017) 145, [[1702.03554](#)].
- [30] B. Fuks, J. H. Kim, and S. J. Lee, *Scrutinizing the Higgs quartic coupling at a future 100 TeV proton-proton collider with taus and b-jets*, *Phys. Lett.* **B771** (2017) 354–358, [[1704.04298](#)].
- [31] M. McCullough, *An Indirect Model-Dependent Probe of the Higgs Self-Coupling*, *Phys. Rev.* **D90** (2014), no. 1 015001, [[1312.3322](#)]. [Erratum: *Phys. Rev.* **D92**, no. 3, 039903 (2015)].
- [32] J. R. Ellis, M. K. Gaillard, and D. V. Nanopoulos, *A Phenomenological Profile of the Higgs Boson*, *Nucl. Phys.* **B106** (1976) 292.
- [33] B. W. Lee, C. Quigg, and H. B. Thacker, *Weak Interactions at Very High-Energies: The Role of the Higgs Boson Mass*, *Phys. Rev.* **D16** (1977) 1519.
- [34] B. L. Ioffe and V. A. Khoze, *What Can Be Expected from Experiments on Colliding e^+e^- Beams with e Approximately Equal to 100-GeV?*, *Sov. J. Part. Nucl.* **9** (1978) 50. [*Fiz. Elem. Chast. Atom. Yadra* **9**, 118 (1978)].
- [35] M. Gorbahn and U. Haisch, *Indirect probes of the trilinear Higgs coupling: $gg \rightarrow h$ and $h \rightarrow \gamma\gamma$* , *JHEP* **10** (2016) 094, [[1607.03773](#)].

- [36] G. Degrandi, P. P. Giardini, F. Maltoni, and D. Pagani, *Probing the Higgs self coupling via single Higgs production at the LHC*, *JHEP* **12** (2016) 080, [[1607.04251](#)].
- [37] W. Bizon, M. Gorbahn, U. Haisch, and G. Zanderighi, *Constraints on the trilinear Higgs coupling from vector boson fusion and associated Higgs production at the LHC*, *JHEP* **07** (2017) 083, [[1610.05771](#)].
- [38] G. Degrandi, M. Fedele, and P. P. Giardini, *Constraints on the trilinear Higgs self coupling from precision observables*, *JHEP* **04** (2017) 155, [[1702.01737](#)].
- [39] G. D. Kribs, A. Maier, H. Rzehak, M. Spannowsky, and P. Waite, *Electroweak oblique parameters as a probe of the trilinear Higgs boson self-interaction*, *Phys. Rev.* **D95** (2017), no. 9 093004, [[1702.07678](#)].
- [40] F. Maltoni, D. Pagani, A. Shivaji, and X. Zhao, *Trilinear Higgs coupling determination via single-Higgs differential measurements at the LHC*, *Eur. Phys. J.* **C77** (2017), no. 12 887, [[1709.08649](#)].
- [41] S. Di Vita, C. Grojean, G. Panico, M. Riembau, and T. Vantalon, *A global view on the Higgs self-coupling*, *JHEP* **09** (2017) 069, [[1704.01953](#)].
- [42] T. Barklow, K. Fujii, S. Jung, M. E. Peskin, and J. Tian, *Model-Independent Determination of the Triple Higgs Coupling at e^+e^- Colliders*, *Phys. Rev.* **D97** (2018), no. 5 053004, [[1708.09079](#)].
- [43] S. Di Vita, G. Durieux, C. Grojean, J. Gu, Z. Liu, G. Panico, M. Riembau, and T. Vantalon, *A global view on the Higgs self-coupling at lepton colliders*, *JHEP* **02** (2018) 178, [[1711.03978](#)].
- [44] D. R. T. Jones and S. T. Petcov, *Heavy Higgs Bosons at LEP*, *Phys. Lett.* **84B** (1979) 440–444.
- [45] C.-S. S. Group, *CEPC-SPPC Preliminary Conceptual Design Report. 1. Physics and Detector*.
- [46] **TLEP Design Study Working Group** Collaboration, M. Bicer *et al.*, *First Look at the Physics Case of TLEP*, *JHEP* **01** (2014) 164, [[1308.6176](#)].
- [47] H. Baer, T. Barklow, K. Fujii, Y. Gao, A. Hoang, S. Kanemura, J. List, H. E. Logan, A. Nomerotski, M. Perelstein, *et al.*, *The International Linear Collider Technical Design Report - Volume 2: Physics*, [1306.6352](#).
- [48] **CLICdp, CLIC** Collaboration, M. J. Boland *et al.*, *Updated baseline for a staged Compact Linear Collider*, [1608.07537](#).
- [49] H. Abramowicz *et al.*, *Higgs physics at the CLIC electron-positron linear collider*, *Eur. Phys. J.* **C77** (2017), no. 7 475, [[1608.07538](#)].
- [50] F. Boudjema and E. Chopin, *Double Higgs production at the linear colliders and the probing of the Higgs selfcoupling*, *Z. Phys.* **C73** (1996) 85–110, [[hep-ph/9507396](#)].
- [51] A. Denner, *Techniques for calculation of electroweak radiative corrections at the one loop level and results for W physics at LEP-200*, *Fortsch. Phys.* **41** (1993) 307–420, [[0709.1075](#)].
- [52] A. A. Sokolov and I. M. Ternov, *On Polarization and spin effects in the theory of synchrotron radiation*, *Sov. Phys. Dokl.* **8** (1964) 1203–1205. [*Phys. Dokl.* 8,1203(1964)].
- [53] **Particle Data Group** Collaboration, C. Patrignani *et al.*, *Review of Particle Physics*, *Chin. Phys.* **C40** (2016), no. 10 100001.

- [54] A. Denner, S. Dittmaier, M. Roth, and M. M. Weber, *Electroweak radiative corrections to $e^+e^- \rightarrow \nu\mu$ anti- $\nu\mu$ H* , *Nucl. Phys.* **B660** (2003) 289–321, [[hep-ph/0302198](#)].
- [55] A. Denner, S. Dittmaier, M. Roth, and M. M. Weber, *Electroweak radiative corrections to single Higgs boson production in e^+e^- annihilation*, *Phys. Lett.* **B560** (2003) 196–203, [[hep-ph/0301189](#)].
- [56] L. Di Luzio, R. Gröber, and M. Spannowsky, *Maxi-sizing the trilinear Higgs self-coupling: how large could it be?*, *Eur. Phys. J.* **C77** (2017), no. 11 788, [[1704.02311](#)].
- [57] J. Tian, *Study of Higgs self-coupling at the ILC based on the full detector simulation at $\sqrt{s}=500$ GeV and $\sqrt{s}=1$ TeV*, in *Helmholtz Alliance Linear Collider Forum: Proceedings of the Workshops Hamburg, Munich, Hamburg 2010-2012, Germany*, (Hamburg), pp. 224–247, DESY, DESY, 2013.
- [58] G. Belanger, F. Boudjema, J. Fujimoto, T. Ishikawa, T. Kaneko, Y. Kurihara, K. Kato, and Y. Shimizu, *Full $O(\alpha)$ electroweak corrections to double Higgs strahlung at the linear collider*, *Phys. Lett.* **B576** (2003) 152–164, [[hep-ph/0309010](#)].
- [59] T. Barklow, K. Fujii, S. Jung, R. Karl, J. List, T. Ogawa, M. E. Peskin, and J. Tian, *Improved Formalism for Precision Higgs Coupling Fits*, *Phys. Rev.* **D97** (2018), no. 5 053003, [[1708.08912](#)].
- [60] H. Abramowicz *et al.*, *The International Linear Collider Technical Design Report - Volume 4: Detectors*, [1306.6329](#).
- [61] A. Sirlin and R. Zucchini, *Dependence of the Quartic Coupling $H(m)$ on $M(H)$ and the Possible Onset of New Physics in the Higgs Sector of the Standard Model*, *Nucl. Phys.* **B266** (1986) 389–409.
- [62] C. Degrande, C. Duhr, B. Fuks, D. Grellscheid, O. Mattelaer, and T. Reiter, *UFO - The Universal FeynRules Output*, *Comput. Phys. Commun.* **183** (2012) 1201–1214, [[1108.2040](#)].
- [63] J. Alwall, R. Frederix, S. Frixione, V. Hirschi, F. Maltoni, O. Mattelaer, H. S. Shao, T. Stelzer, P. Torrielli, and M. Zaro, *The automated computation of tree-level and next-to-leading order differential cross sections, and their matching to parton shower simulations*, *JHEP* **07** (2014) 079, [[1405.0301](#)].
- [64] T. Hahn, *Generating Feynman diagrams and amplitudes with FeynArts 3*, *Comput. Phys. Commun.* **140** (2001) 418–431, [[hep-ph/0012260](#)].
- [65] T. Hahn and M. Perez-Victoria, *Automatized one loop calculations in four-dimensions and D-dimensions*, *Comput. Phys. Commun.* **118** (1999) 153–165, [[hep-ph/9807565](#)].
- [66] R. K. Ellis and G. Zanderighi, *Scalar one-loop integrals for QCD*, *JHEP* **02** (2008) 002, [[0712.1851](#)].
- [67] S. Carrazza, R. K. Ellis, and G. Zanderighi, *QCDLoop: a comprehensive framework for one-loop scalar integrals*, *Comput. Phys. Commun.* **209** (2016) 134–143, [[1605.03181](#)].